

(NASA-CR-165561) STRESS EVALUATIONS UNDER
ROLLING/SLIDING CONTACTS Final Report
(Battelle Columbus Labs., Ohio.) 54 p
HC A04/UF A01 CSCI 20K

NASA CR 165561

N82-17521

FINAL REPORT

G3/39

Unclass
08966

ON

STRESS EVALUATIONS UNDER ROLLING/SLIDING CONTACTS

to

NASA

NATIONAL AERONAUTICS AND SPACE ADMINISTRATION
LEWIS RESEARCH CENTER
CLEVELAND, OHIO 44135

October 30, 1981

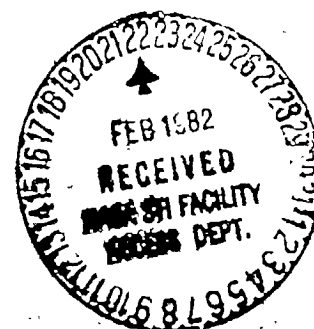
by

J. W. Kannel
and
J. L. Tevaarwerk (Consultant)



Battelle

Columbus Laboratories
505 King Avenue
Columbus, Ohio 43201



1 Report No NASA CR-165561		2 Government Accession No		3 Recipient's Catalog No	
4 Title and Subtitle Stress Evaluations Under Rolling/Sliding Contacts				5 Report Date October 30, 1981	
				6 Performing Organization Code	
7 Author(s) J. W. Kannel and J. L. Tevznerwerk				8 Performing Organization Report No G7782	
9 Performing Organization Name and Address Battelle-Columbus Laboratories 505 King Avenue Columbus, Ohio 43201				10 Work Unit No	
				11 Contract or Grant No NAS 3-22808	
12 Sponsoring Agency Name and Address				13 Type of Report and Period Covered Contractor's Report	
				14 Sponsoring Agency Code	
15 Supplementary Notes Final Report. Project Manager, S. Loewenthal; Bearing, Gearing, and Transmission Section, NASA-Lewis Research Center, Cleveland, Ohio 44135.					
16 Abstract Computer models have been developed for analyzing the state-of-stress beneath traction-drive type of contacts. The analyses involve computing stresses and stress-reversals on various planes for points beneath the surface. The effect of tangential and axial friction under gross slip conditions can be evaluated with the models. Evaluations performed on an RC (rolling contact) tester configuration indicate that the classical fatigue stresses are not altered by friction-forces typical of lubricated contact. Higher values of friction ($f > 0.25$) can result in surface shear reversal that exceeds the stresses at the depth of maximum shear reversal under rolling contact.					
17 Key Words (Suggested by Author(s)) Traction Drives, Traction Contacts, Reliability, Stress Analysis, Friction, Fatigue Life, Lubrication			18 Distribution Statement Unclassified - Unlimited		
19 Security Classif. (of this report) Unclassified		20 Security Classif. (of this page) Unclassified		21 No. of Pages 50	
				22 Price*	

* For sale by the National Technical Information Service, Springfield, Virginia 22161

TABLE OF CONTENTS

	<u>Page No.</u>
INTRODUCTION	1
MODEL DEVELOPMENT.	5
The Stress Tensor.	5
Principal Stresses	7
Angles to the Principal Stresses	9
Other Planes of Interest	9
Plane of Maximum Shear Stress	10
Plane of Octahedral Stress.	10
Seeking the Maximum and Minimum Shear Stresses	11
Construction of Model.	12
ANALYSIS FOR RC FATIGUE TESTER	14
DISCUSSION OF EFFECTS OF FRICTION ON FATIGUE STRESSES.	17
SUMMARY.	30
REFERENCES	31
APPENDIX A: COMPUTATIONS OF THE STRESS TENSOR	A-1
APPENDIX B: SOURCE LISTING FOR BATTELLE STRESS MODEL.	B-1

LIST OF FIGURES

FIGURE 1.	Illustration of Shear Stress Beneath the Surface of Contact	3
FIGURE 2.	Contact Between Rolling/Sliding Bodies	6
FIGURE 3.	Pressure Ellipse	6
FIGURE 4.	Illustration of Axis Rotation.	8
FIGURE 5.	Effect of Friction on Reversing Shear Stress for RC Tester ($K = .8$, $\nu = .285$, B-Model).	15
FIGURE 6.	Effect of Friction on Reversing Orthogonal Shear Stress ($K = 0$, $\nu = .285$, $z/b = .5$, T-Model).	18

LIST OF FIGURES
(Continued)

	<u>Page No.</u>
FIGURE 7. Effect of Friction on Reversing Orthogonal Shear Stress ($K = .5$, $\nu = .285$, $z/b = .435$, T-Model) . . .	19
FIGURE 8. Effect of Friction on Reversing Orthogonal Shear Stress ($K = 1$, $\nu = .285$, $z/b = .35$, T-Model)	20
FIGURE 9. Effect of Aspect Ratio k on Reversing Orthogonal Shear Stress ($f_T = f_A = 0$, $\nu = .285$, T-Model	21
FIGURE 10. Effect of Aspect Ratio on Reversing Orthogonal Shear Stress ($f_T = .2$, $\nu = .285$, T-Model).	22
FIGURE 11. Effect of Friction on Magnitude of Maximum Shear Stress (T-Model)	23
FIGURE 12. Effect of Friction on Depth of Maximum Shear Stress (T-Model)	24
FIGURE 13. Effect of Friction on Maximum Octahedral Shear Stress (T-Model)	26
FIGURE 14. Effect of Friction on Depth of Maximum Octahedral Stress.	27
FIGURE 15. Effect of Friction on Maximum Stress Reversals ($K = 0$, $f_A = 0$, $\nu = .285$, B-Model)	28
FIGURE 16. Illustration on Variation of Shear Stress on Plane of Maximum Shearing Stress ($z/b = 0$, $K = 0$, $\nu = .25$, $f_T = .333$, T-Model).	29

LIST OF TABLES

TABLE 1. Comparison of Tevaarwerk Model with Battelle Model	4
TABLE 2. Typical Printout for Battelle Stress Model	13

ABSTRACT

Computer models have been developed for analyzing the state-of-stress beneath traction-drive type of contacts. The analyses involve computing stresses and stress-reversals on various planes for points beneath the surface. The effect of tangential and axial friction under gross slip conditions can be evaluated with the models. Evaluations performed on an RC (rolling contact) tester configuration indicate that the classical fatigue stresses are not altered by friction-forces typical of lubricated contact. Higher values of friction ($f > 0.25$) can result in surface shear reversal that exceeds the stresses at the depth of maximum shear reversal under rolling contact.

STRESS EVALUATIONS UNDER ROLLING/SLIDING CONTACTS

by

J. W. Kannel and J. L. Tevaarwerk (Consultant)

INTRODUCTION

Rolling elements such as roller bearings and traction drive transmissions are subject to failure from rolling contact fatigue. Such fatigue failures cause a serious restriction on the operating life and reliability of such devices. In the case of the traction drive transmissions, rolling contact fatigue failures could conceivably restrict the use of such transmissions in motor vehicles, despite the increased efficiency such transmissions could afford. Although a number of factors contribute to fatigue failure, the effect of traction and slip on the state of stress between rolling elements is not understood. A better understanding of the role of traction on fatigue could greatly assist in the evaluation of materials for and operational limits of traction components.

The fundamental theory for rolling contact fatigue is the one published by Lundberg and Palmgren^{(1)*} in 1947 and summarized by Coy, et al.⁽²⁾. This theory is based on the assumption that failure is in the form of shallow pitting and is related to subsurface shearing stresses within the rolling elements. In essence, any irregularity in the material beneath the surface can manifest itself as a failure initiation point. The significant stress field has been hypothesized as being bounded by the surface, the depth of the maximum and reversing shear stress, and the width of the rolling track. The magnitude and depth of the reversing shear stress have been found to be very significant with regards to fatigue failure.

The reversing stress field has been well established for pure rolling contacts^(3,4). However, when surface tractions are imposed, this stress field becomes very complicated. The classic study for line contact is by Smith and Liu⁽⁵⁾. Smith and Liu's research indicated that friction is a key

*References are listed at the end of the text.

factor with regards to reversing stresses. For example, at some level of friction, the reversing stress was found to be at the surface, which would greatly reduce fatigue life. Hamilton and Goodman⁽⁶⁾ developed a theory for a circular sliding contact. The results of their theory are in the form of useful graphs for predicting friction effects for this specific type of contact. Other researchers, such as Kuznetsov⁽⁷⁾, have studied the influence of friction on contact stress, but not on the subsurface stress field under slip conditions.

One complication to the reversing stress field is that the stress reversals occur over the width of contact and depend on orientation as well as depth. See, for example, Figure 1. The maximum stress occurs at the center of contact and the depth and magnitude are straightforward to compute. Computing the reversing stress becomes more complicated because the reversals occur over a finite region. Consider, then, the complication when the magnitude of τ_+ or τ_- depend on the orientation out of the plane of the paper.

The goal of the project has been to develop computer models to determine the magnitude of reversing shear stresses beneath (and very near) the surface of rolling/sliding contacts. Sliding in both the tangential direction and the axial direction are considered. Considerations are given for line contacts as well as crowned rollers. In order to insure accuracy in modeling, two independent models were developed, one by Tevaarwerk (T-model) and one at Battelle (B-model)*. This approach allowed for both researchers to be heavily involved with the problem in modeling and created excellent dialogue, both for the mathematical intricacies, as well as the ramification of the predictions. A comparison between the two models is given in Table 1, which demonstrates the consistency of the two approaches. The approach for the development of the models was as follows:

- Define the stress tensor for any point beneath the surface
- Compute principal stresses and their direction cosines for each point
- Determine the direction cosines (relative to the x, y, z axes) to the octahedral plane and the plane of maximum shearing stress

*As discussed in Appendix A, the primary difference in the two models is in the integration scheme used to determine the stress tensor.

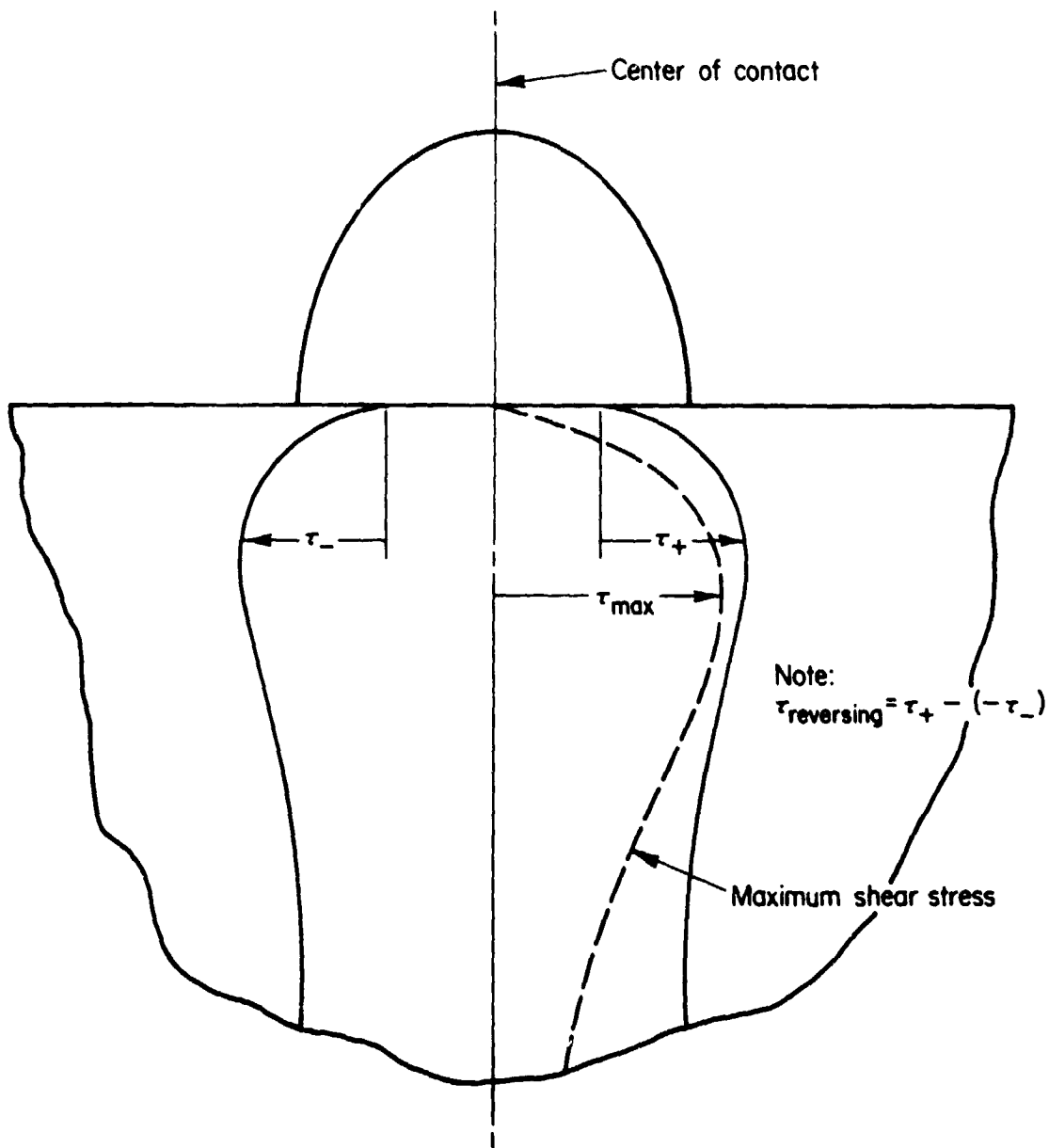


FIGURE 1. ILLUSTRATION OF SHEAR STRESS BENEATH THE SURFACE OF CONTACT

TABLE 1. COMPARISON OF TEVAARWERK MODEL WITH BATTELLE MODEL
 ($K = .5$, $\nu = .285$, $f_A = 0$, $z/b = .3$)

f_T	z/b	σ_x		σ_y		σ_z		τ_{xy}		τ_{yz}		τ_{xz}	
		T	B	T	B	T	B	T	B	T	B	T	B
0	-.9	-.236	-.241	-.212	-.218	-.375	-.383	0	0	0	0	.228	.231
	-.8	-.251	-.256	-.255	-.259	-.511	-.518	0	0	0	0	.222	.225
	-.5	-.329	-.333	-.361	-.369	-.798	-.807	0	0	0	0	.138	.140
	-.3	-.374	-.380	-.404	-.412	-.896	-.907	0	0	0	0	.080	.081
	0	-.401	-.408	-.428	-.436	-.948	-.958	0	0	0	0	0	0
	.3	-.374	-.380	-.404	-.412	-.896	-.907	0	0	0	0	-.080	-.081
	.5	-.329	-.333	-.361	-.369	-.798	-.807	0	0	0	0	-.138	-.141
	.8	-.251	-.256	-.255	-.259	-.511	-.518	0	0	0	0	-.222	-.225
	.9	-.236	-.240	-.212	-.218	-.375	-.383	0	0	0	0	-.228	-.230
.1	-.9	-.171	-.174	-.196	-.201	-.352	-.360	0	0	0	0	.195	.200
	-.8	-.188	-.191	-.239	-.243	-.489	-.495	0	0	0	0	.187	.190
	-.5	-.281	-.284	-.349	-.356	-.784	-.793	0	0	0	0	.095	.097
	-.3	-.344	-.349	-.396	-.414	-.888	-.898	0	0	0	0	.032	.033
	0	-.401	-.408	-.428	-.436	-.948	-.958	0	0	0	0	-.051	-.051
	.3	-.404	-.411	-.412	-.420	-.904	-.915	0	0	0	0	-.128	-.130
	.5	-.376	-.382	-.373	-.381	-.812	-.821	0	0	0	0	-.182	-.184
	.8	-.315	-.320	-.271	-.276	-.533	-.540	0	0	0	0	-.256	-.260
	.9	-.301	-.308	-.228	-.234	-.398	-.406	0	0	0	0	-.260	-.264

- Scan the planes of octahedral and maximum shearing stress in the direction of rolling and compute stress reversals.

Stress reversals can be computed by the above procedure for conditions of zero friction, axial friction, and tangential friction for line contacts and contacts corresponding to a rolling contact fatigue tester. The basic assumptions for the analyses are:

1. The contact pressure (normal stress) are predictable by Hertz theory for line or crowned contacts.
2. The contact tractions are a result of a constant traction coefficient times the pressure. This tacitly assumes a gross sliding situation.
3. The materials are all elastic and homogeneous.
4. The bodies are isothermal. That is, no thermal stresses are considered.

MODEL DEVELOPMENT

The Stress Tensor

The objective of the analyses is to evaluate subsurface stresses in rolling/sliding contacts of the type seen in traction drives. Consider, for example, the system shown in Figure 2, where two cylinders are loaded together under rolling or possibly rolling/sliding contact. The assumed Hertzian contact pressure distribution produces a state of stress throughout the cylinders. Likewise, the frictional forces associated with sliding produce an additional state of stress such that a typical point beneath the surface is undergoing a complicated and changing stress state. For crowned cylinders, this stress state varies axially (in the y direction) as a result of axially varying pressures as well as in the x direction, as shown in Figure 3.

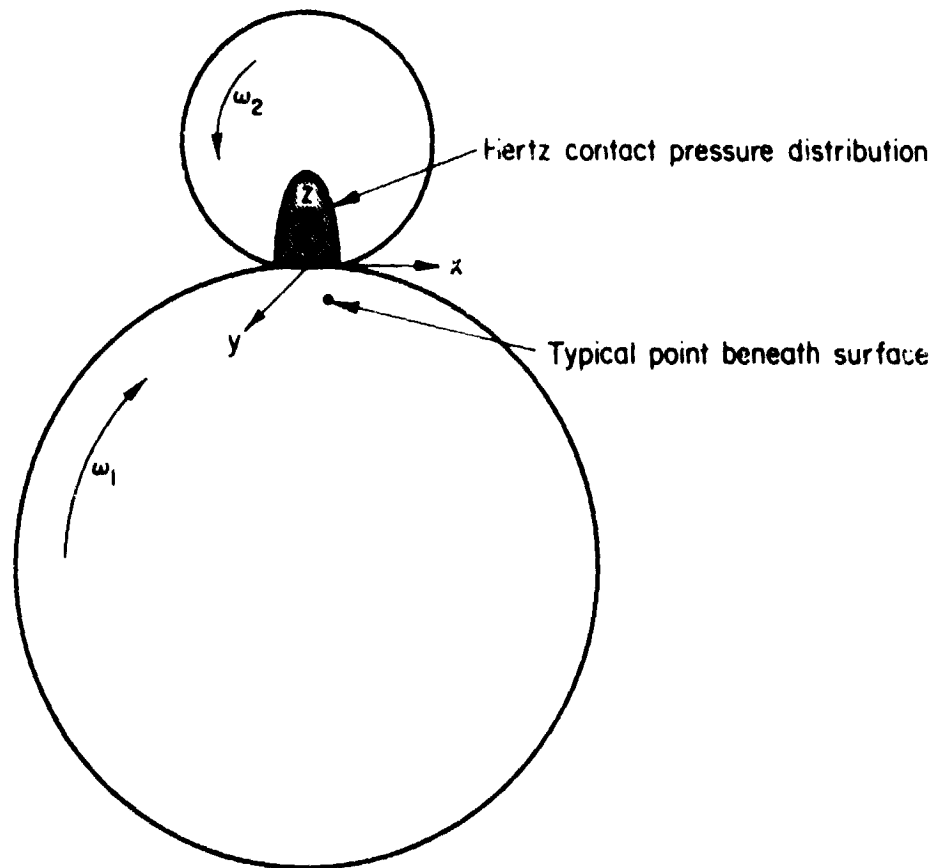


FIGURE 2. CONTACT BETWEEN ROLLING/SLIDING BODIES

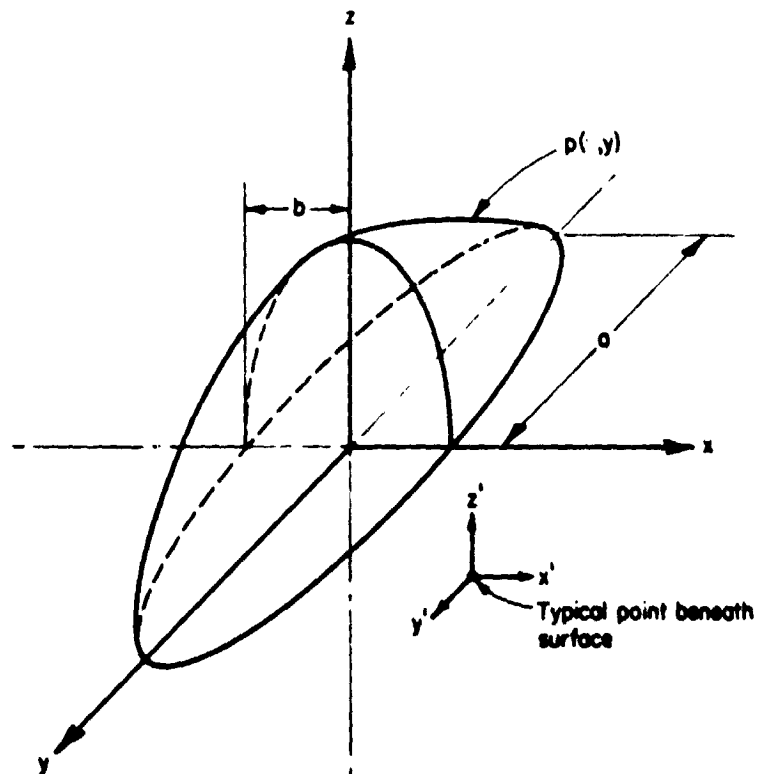


FIGURE 3. PRESSURE ELLIPSE

In tensor notation, the stress at any point can be written as

$$\sigma_{ij} \quad \text{or} \quad \bar{\sigma}_{ij} , \quad (1)$$

where $\bar{\sigma}_{ij} = \sigma_{ij}/p_H \quad (i, j = 1, 2, 3) ,$

where p_H is the maximum Hertz contact pressure. In more conventional terminology

$$\begin{aligned} \sigma_x &= \sigma_{11} , \quad \sigma_y = \sigma_{22} , \quad \sigma_z = \sigma_{33} , \\ \tau_{xy} &= \sigma_{12} , \quad \tau_{xz} = \sigma_{13} \text{ and } \tau_{yz} = \sigma_{23} . \end{aligned} \quad (2)$$

It should be noted that the stress tensor is symmetric such that $\sigma_{ij} = \sigma_{ji}$.

To determine σ_{ij} requires that expressions be developed for the effect of point loads on stresses and that the point loads be integrated over the conditions of interest. These equations are discussed in Appendix A and Equation A-27 shows the general relationship for $\bar{\sigma}_{ij}$ of interest here.

Principal Stresses

From the preceding discussions, it can be noted that the state of stress at any point has six components*. The components discussed in the preceding section describe the stress when the axis is oriented in the x, y, z system. However, the stress can look considerably different at different orientations. Since the objective of the study is to evaluate "worst case" shear stresses, it is necessary to evaluate the effect of axis rotation (see Figure 4) on stress. The first step in this phase of the study is to determine the parameters that are not a function of rotation; these are known as the invariants of the stress tensor⁽⁸⁾. These invariants are:

*Actually nine components are required, but some are equal because of symmetry.

$$I_r = \sigma_{11} + \sigma_{22} + \sigma_{33} \quad , \quad (3)$$

$$II_r = \sigma_{11} \sigma_{22} + \sigma_{11} \sigma_{33} + \sigma_{22} \sigma_{33} - \sigma_{12}^2 - \sigma_{13}^2 - \sigma_{23}^2 \quad , \text{ and} \quad (4)$$

$$III_r = \sigma_{11} \sigma_{22} \sigma_{33} + 2\sigma_{12} \sigma_{23} \sigma_{13} - \sigma_{11} \sigma_{23}^2 - \sigma_{22} \sigma_{13}^2 - \sigma_{33} \sigma_{12}^2 \quad . \quad (5)$$

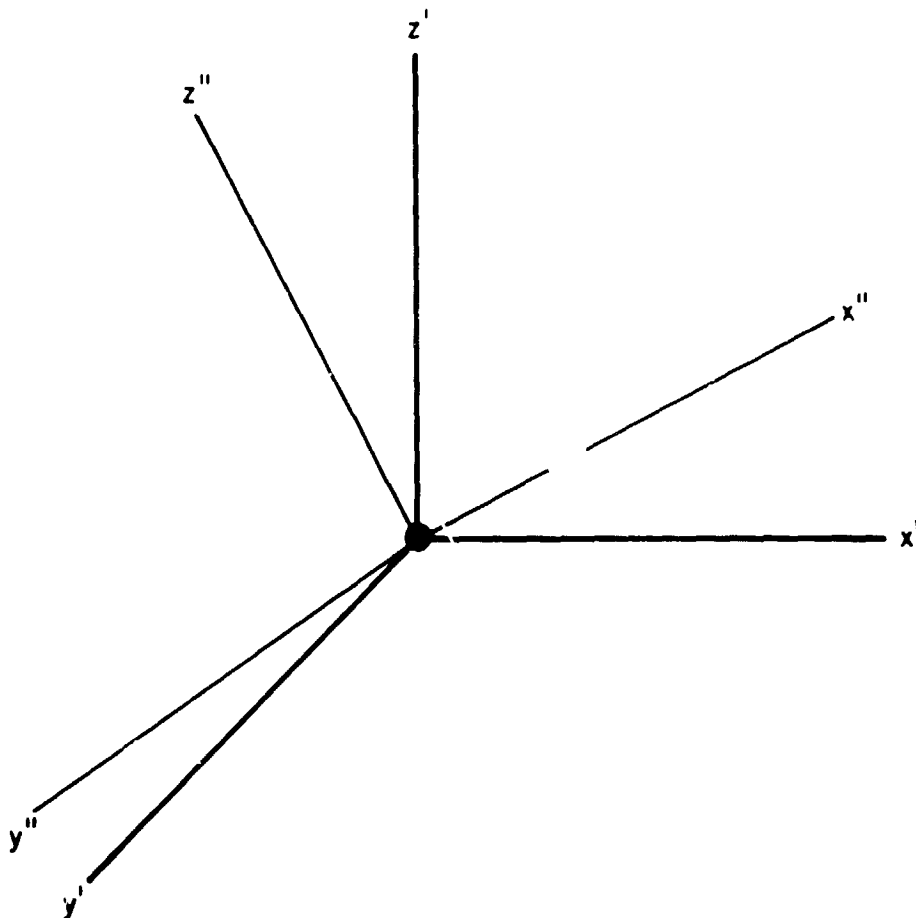


FIGURE 4. ILLUSTRATION OF AXIS ROTATION

With the knowledge of the invariants, it is possible to determine the plane of the principal stress (i.e., the rotated axis on which no shear forces exist) and the stress magnitudes. The equations for the principal stresses can be written

$$S^3 + I_r S^2 + II_r S + III_r = 0 \quad . \quad (6)$$

Equation 6 can be readily solved by cubic equation solutions and will produce three real roots for principal stresses. These roots will be known as S_1 , S_2 , and S_3 with S_1 being the largest and S_3 the smallest.

Angles To The Principal Stresses

In tensor computations, the angles are given in terms of direction cosines to the various axes. If we define a_{nx} , a_{ny} , and a_{nz} as the direction cosines from a given principal stress (say S_1) to the x, y, and z axis, then it can be shown that the following equations must be satisfied⁽⁸⁾:

$$a_{nx1}^2 + a_{ny1}^2 + a_{nz1}^2 = 1 \quad , \quad (7)$$

$$(\sigma_{11} - S_1) a_{nx1} + \sigma_{12} a_{ny1} + \sigma_{13} a_{nz1} = 0 \quad , \quad (8)$$

$$\sigma_{12} a_{nx1} + (\sigma_{22} - S_1) a_{ny1} + \sigma_{23} a_{nz1} = 0 \quad , \text{ and} \quad (9)$$

$$\sigma_{13} a_{nx1} + \sigma_{23} a_{ny1} + (\sigma_{33} - S_1) a_{nz1} = 0 \quad . \quad (10)$$

By solving Equation 7 and any two of Equations 8 through 10 simultaneously, a_{nx1} , a_{ny1} and a_{nz1} can be determined. In a like manner, the direction cosines for locating the S_2 (a_{nx2} , a_{ny2} , a_{nz2}) and the S_3 (a_{nx3} , a_{ny3} , a_{nz3}) stress can be determined.

Other Planes of Interest

The solution of equation 7 through 10 permit the determination of the location of principal stresses. However, the objective of the project is to evaluate shear stresses and by definition there are no shear stresses on these planes. Therefore, other planes must be considered.

Plane of Maximum Shear Stress

The maximum shear stress for an element lies on a plane bisecting the $S_1 - S_3$ plane. The direction cosines for the normal to this plane relative to the plane of the principal stress axes can be written

$$b_{n1} = 1/\sqrt{2} , \quad (11)$$

$$b_{n2} = 0. , \quad (12)$$

$$b_{n3} = 1/\sqrt{2} . \quad (13)$$

To relate these cosines back to the x, y, z axis requires an angle transformation of the form

$$c_{nx} = b_{n1} a_{nx1} + b_{n2} a_{nx2} + b_{n3} a_{nx3} , \quad (14)$$

$$c_{ny} = b_{n1} a_{ny1} + b_{n2} a_{ny2} + b_{n3} a_{ny3} , \quad (15)$$

$$c_{nz} = b_{n1} a_{nz1} + b_{n2} a_{nz2} + b_{n3} a_{nz3} , \quad (16)$$

where c_{n1} , c_{n2} and c_{n3} are the direction cosines from the normal (to the shear plane) to the x, y, z axes.

Plane of Octahedral Stress

The location of the normal to the octahedral stress can be written

$$b_{n1} = 1/\sqrt{3} , \quad (17)$$

$$b_{n2} = 1/\sqrt{3} , \quad (18)$$

$$b_{n3} = 1/\sqrt{3} . \quad (19)$$

That is, the normal is situated at equal angles from the principal axis. Likewise, Equations 17 through 19 can be used in conjunction with Equations 14 through 16 to relate the normal to the x, y, z axes.

Seeking The Maximum and Minimum Shear Stresses

Using the angle transformation equations discussed in the previous section, it is possible to locate the normals to various critical shear stress planes. The final step in this process is to locate maximum and minimum shear stress on those particular planes for various x positions. Let us define the direction cosines to a given location on a shear plane as a_{sx} , a_{sy} and a_{sz} . It can be shown that⁽⁸⁾

$$a_{sx} c_{nx} + a_{sy} c_{ny} + a_{sz} c_{nz} = 0 \quad \text{and} \quad (20)$$

$$a_{sx}^2 + a_{sy}^2 + a_{sz}^2 = 1 \quad . \quad (21)$$

If, then, we choose a particular angle, say a_{sx} , we can compute a_{sy} and a_{sz} by Equations 20 and 21.

With a knowledge of the angles between the shear vector on a plane and the x , y , z axes and a knowledge of the stress tensor as oriented to the x , y , z axes, the shear stress can be computed. The equation for the stress is given by⁽⁸⁾

$$\begin{aligned} \tau = & c_{nx} a_{sx} \sigma_{11} + c_{ny} a_{sy} \sigma_{22} + c_{nz} a_{sz} \sigma_{33} \quad , \\ & + c_{nx} a_{sy} \sigma_{12} + c_{ny} a_{sx} \sigma_{21} + c_{nx} a_{sz} \sigma_{13} \quad , \\ & + c_{nz} a_{sx} \sigma_{31} + c_{ny} a_{sz} \sigma_{23} + c_{nz} a_{sy} \sigma_{32} \quad . \end{aligned} \quad (22)$$

In the computer model, values of a_{sx} were assumed in the range -1 to $+1$. For each value of a_{sx} , the shear stress was computed at various x positions and both the maximum and minimum values were stored. In the computation, the maximum shear stress and the maximum reversal $\tau_{\max} - \tau_{\min}$ were sought.

Construction Of Model

The computer model is constructed as follows:

1. Input values of λ (b/a), ν (Poissons ratio), z/b (depth) f_T (tangential friction coefficient), f_A (axial friction coefficient), and case number.
2. Compute the stress tensor for approximately eleven (11) x locations (STRSSC). For $K = 0$ (line contact), the Smith-Liu⁽⁵⁾ solutions are used.
3. Compute the principal stresses at each x location (PRINC).
4. Compute the angles to the principal stresses at each location (ANGLP).
5. Compute the angle to the normals of the maximum shear plane, the octahedral shear plane, and the orthogonal plane (ANGTRAN).
6. Compute the shear stresses and shear reversals on the shear planes (RVSTRS).

All computations are in the form σ_{ij}/p_H and are applicable for any (elastic) contact pressure level. A source listing for the model is given in Appendix B and a typical printout is given in Table 2.

In this table

$K = b/a$ (aspect ratio)

$\nu =$ (Poissons ratio)

$Z = z/b$ (depth into surface)

$F_T = f_T$ (tangential friction coefficient)

$F_A = f_A$ (axial friction coefficient)

S_{XX}, S_{YY}, S_{ZZ} are the normal stresses ($\sigma_x, \sigma_y, \sigma_z$)

S_{XY}, S_{YZ}, S_{XZ} are the shear stress ($\tau_{xy}, \tau_{yz}, \tau_{xz}$)

S_1, S_2, S_3 are the principal stresses

$X - pos = x/b$ is the x position being evaluated

$\tau_{MAX} =$ maximum shearing stress as computed by scanning different planes

$AN(1), AN(2), AN(3)$ are the direction cosines to the normals on the planes containing τ_{MAX} and, $AS(1), AS(2), AS(3)$ are the direction cosines to τ_{MAX} on the shear plane.

TABLE 2. TYPICAL PRINTOUT FOR BATTELLE STRESS MODEL

CASE NUMBER= 100

K= .80000E+00 MU= .28500E+00 L= .10000E+00 FT= .10000E+00 FA= 0.

IX	SXX	SYX	SZZ	SXY	SVZ	SNZ	S1	S2	S3	K-PDS
1	-.59283E-01	-.17261E+00	-.13866E+00	.35355E-08	.35355E-08	.11783E+00	.25361E-01	-.17262E+00	-.22331E+00	-.10000E+01
2	-.11560E+00	-.26274E+00	-.39002E+00	.3521E-08	.35213E-08	.11627E+00	-.72964E-01	-.26274E+00	-.43265E+00	-.90000E+00
3	-.21121E+00	-.34511E+00	-.56935E+00	.35295E-08	.35295E-08	.77624E-01	-.19519E+00	-.34511E+00	-.28538E+00	-.80000E+00
4	-.45779E+00	-.51183E+00	-.85828E+00	.35244E-08	.35244E-08	-.10770E-01	-.45750E+00	-.51183E+00	-.85855E+00	-.50000E+00
5	-.56596E+00	-.57347E+00	-.95228E+00	.35446E-08	.35446E-08	-.45295E-01	-.56072E+00	-.57347E+00	-.95752E+00	-.30000E+00
6	-.65376E+00	-.61313E+00	-.10029E+01	.35196E-08	.35196E-08	-.81005E-01	-.61313E+00	-.63588E+00	-.10208E+01	0.
7	-.65600E+00	-.59489E+00	-.95857E+00	.35446E-08	.35446E-08	-.10808E+00	-.59489E+00	-.62136E+00	-.99321E+00	.30000E+00
8	-.60578E+00	-.54672E+00	-.86971E+00	.35244E-08	.35244E-08	-.12563E+00	-.54672E+00	-.55554E+00	-.91995E+00	.50000E+00
9	-.42607E+00	-.39441E+00	-.59386E+00	.35295E-08	.35295E-08	-.16825E+00	-.32196E+00	-.39441E+00	-.69797E+00	.80000E+00
10	-.33809E+00	-.31191E+00	-.41976E+00	.35213E-08	.35213E-08	-.18799E+00	-.18655E+00	-.31191E+00	-.57129E+00	.90000E+00
11	-.26966E+00	-.21612E+00	-.16702E+00	.35355E-08	.35355E-08	-.17406E+00	-.36877E-01	-.21612E+00	-.39981E+00	.10000E+01

FATIGUE SHEAR STRESS SUMMARY

PLANE OF MAX SHEAR STRESS

TAU MAX= .20372E+00 AN(1)= -.21583E+00 AN(2)= .70711E+00 AN(3)= -.67337E+00 X-REF= .30000E+00
 TAU REVERSING= .32192E+00 AS(1)= -.10000E+00 AS(2)= -.70200E+00 AS(3)= -.70512E+00

PLANE OF MAX OCT SHEAR STRESS

TAU MAX= .20014E+00 AN(1)= -.18715E+00 AN(2)= .57735E+00 AN(3)= .79476E+00 X-REF= .80000E+00
 TAU REVERSING= .27615E+00 AS(1)= -.50000E+00 AS(2)= .64042E+00 AS(3)= -.58297E+00

PLANE OF REVERSING SHEAR STRESS

TAU MAX= .18799E+00 AN(1)= 0. AN(2)= 0. AN(3)= .10000E+01 X-REF= .REF=
 TAU REVERSING= .30582E+00 AS(1)= -.10000E+01 AS(2)= 0. AS(3)= 0.

TAU-REVERSING is the maximum reversing shear stress on the planes specified.

ANALYSIS FOR RC FATIGUE TESTER

One objective of the project has been to evaluate the effect of magnitude and direction of slip on the stresses in a rolling contact (RC) fatigue tester. The RC tester consists of a rotating cylindrical specimen loaded between two large diameter crowned rollers. In the test, the specimen is driven by an electric motor; the crowned rollers are only driven by the specimen. The rollers are loaded to a level to produce fatigue in the specimen in a reasonable time period. Normally, the RC tester is used to evaluate rolling contact fatigue and has been used in bearing-material evaluations. The tester is also being considered as a candidate device for evaluating the effect of friction on fatigue.

Two approaches could be used to induce friction between the cylindrical specimen and the crowned rollers. One technique would be to induce a drag between the two elements by driving or braking the rollers. This approach could be quite complicated for simple fatigue testing and an alternate could be more desirable. This alternate approach could consist simply of skewing the specimen relative to the rollers. However, skewing produces an axial traction, whereas braking the rollers produces a tangential traction. The stress model can be used in determining the stress fields associated with these two types of fatigue test concepts.

Typical dimensions for an RC rig are

$$D_s = 9.5 \text{ mm (0.375 inch)}$$

$$D_r = 190 \text{ mm (7.5 inches)}$$

$$R_c = 6.4 \text{ mm (0.25 inch)}.$$

D_s is the specimen diameter, D_r is the roller diameter, and R_c is the crown radius. For these dimensions, a value of $K = 0.8$ has been computed. The upper limit traction coefficient should be nominally 0.1 for lubricated tractions.

Figure 5 shows the effect of traction on the reversing shear stresses in the RC tester. As can be observed, the maximum stress is unaffected by the

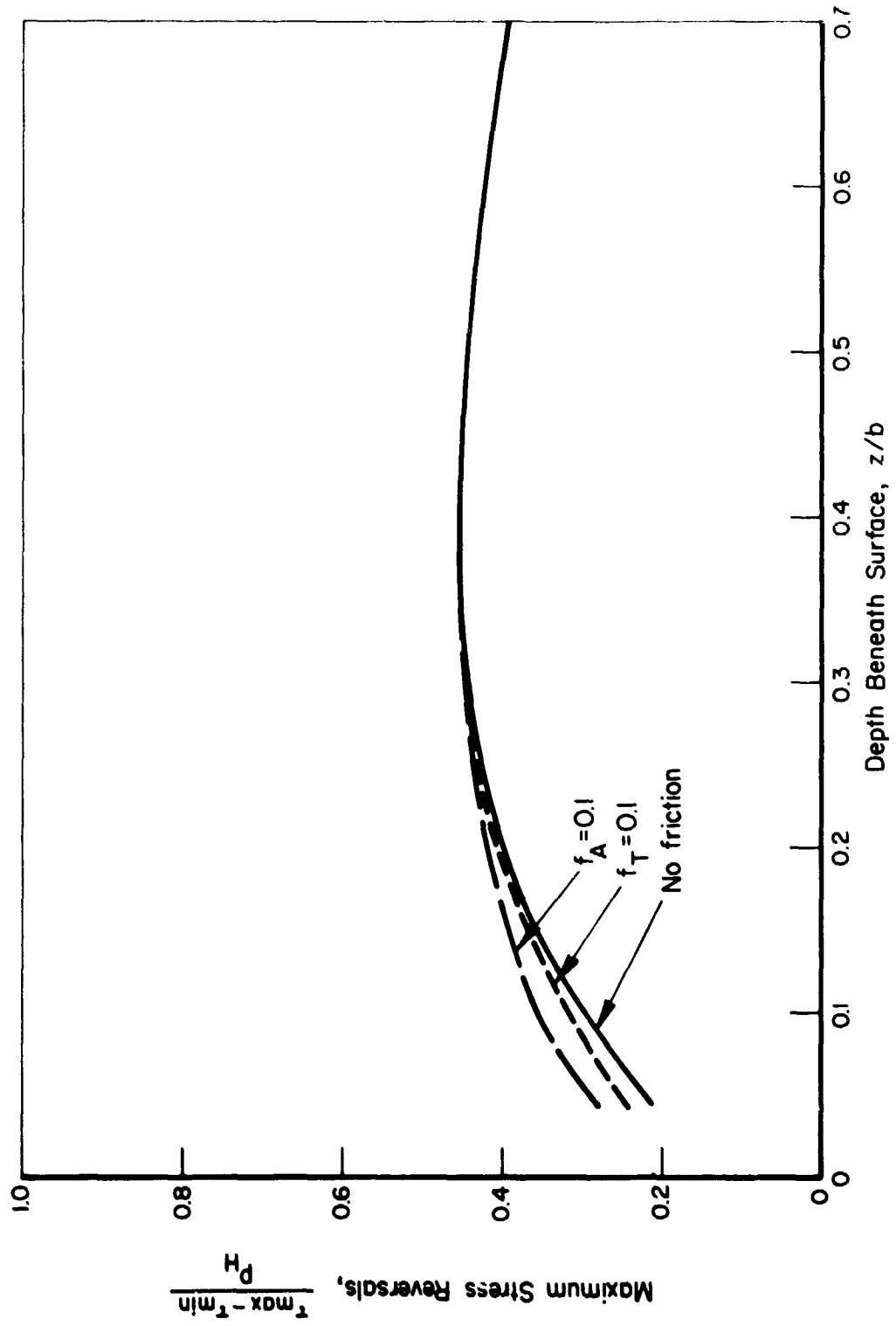


FIGURE 5. EFFECT OF FRICTION ON REVERSING SHEAR STRESS FOR RC TESTER
 ($K = .8$, $\nu = .285$, B-Model)

friction as is the depth to maximum stress ($z/b = 0.38$). There are some differences in the stresses near the surface, and it is impossible to be certain how these differences affect life. However, in the Lundberg-Palmgren theory, only the orthogonal shear reversal and its depth are important. If this theory is valid, it says that a traction coefficient of up to 0.1 should not alter life. There is, however, a difference in off-set between axial and tangential-friction, but this effect is not a part of fatigue theory. Fatigue tests are badly needed to clarify the effect of stress on life.

The general observation from this aspect of the analyses is that the direction of the traction is not significant with regards to fatigue type stress for low traction coefficients typical of lubricated contacts assuming Lundberg-Palmgren's theory. It should be noted that at least three stress related factors that have not been included in these stress analyses could have a profound effect on fatigue. These factors are:

- (1) the effect of temperature (due to friction) on stress
- (2) the effect of non-Hertzian pressure on stress
- (3) the effect of asymmetric surface traction.

All of these can produce an asymmetry in stresses which can amplify the stress reversal. In fact, there will be a different stress state in the driver and driven for effects (1) and (3). The influence of the non-Hertzian pressure should be the same on both bodies provided that we do not invoke hysteresis effects in the material.

If we examine the influence of (1) and (3) on, say, the reversing orthogonal stress and assume that the traction is caused by the shearing of an elastic/plastic-like material, then the surface traction in the latter half of the contact is larger than in the front. Also the traction stresses will be negative in direction on the driver and positive on the driven. This means that the stress reversal in the driven is increased from the non-traction condition while it is decreased in the driver, possibly explaining some of the experimental findings reported elsewhere. The depth at which the maximum orthogonal acts is also reduced by an asymmetric traction stress. Traction produced by an elastic/plastic-like material may also explain why gears fail by pitting fatigue in the region directly below the pitch circle because the positive sliding conditions may produce a region of maximum surface traction

asymmetry and, hence, the largest magnitude of the reversing orthogonal shear stress. The thermal stresses produced by the sliding would also alter the stress profile for the orthogonal shear stress in a similar fashion but now because the driver (i.e., the faster moving body) would see a lower flash temperature than the driven. Thermal stresses would tend to increase the orthogonal shear stress in both bodies but more in the driven than the driver. Also besides the increases in the amplitude of the stress reversal, the depth at which this occurs is reduced, giving a further reduction in fatigue life on the driver. Further research is needed in this area to establish the influence of the effects just mentioned.

DISCUSSION OF EFFECTS OF FRICTION ON FATIGUE STRESSES

The subsurface stress model represents a useful tool for evaluating the role of friction on fatigue type stresses. The results of the evaluations of the stress analyses from the RC tester showed some interesting (although perhaps not profound) implications of the effect of lubricated traction on stresses. The purpose of this section is to further explore the effect of friction on stress.

Figures 6 through 8 show predictions of the reversing orthogonal shear stress for various conditions of friction and aspect ratio (b/a). This reversing stress is normally considered the significant stress for fatigue.⁽¹⁾ Note, however, in Figure 6, that friction does not alter the magnitude of the difference between maximum and minimum shear stress (i.e., stress reversals). This implies that the magnitude of the orthogonal stress reversals are not dependent on friction. Changing aspect ratio does alter the magnitude of the stress as shown in Figures 9 and 10, but this dependence of stress on aspect ratio is not affected by friction.

The effects of friction on the magnitude and depth of the maximum shear stress, are shown in Figures 11 and 12 for various values of aspect ratio. Some increase in stress accompanies an increase in friction. However, for $f_T = .1$ and $\nu = .285$ which are reasonable values for lubricated traction

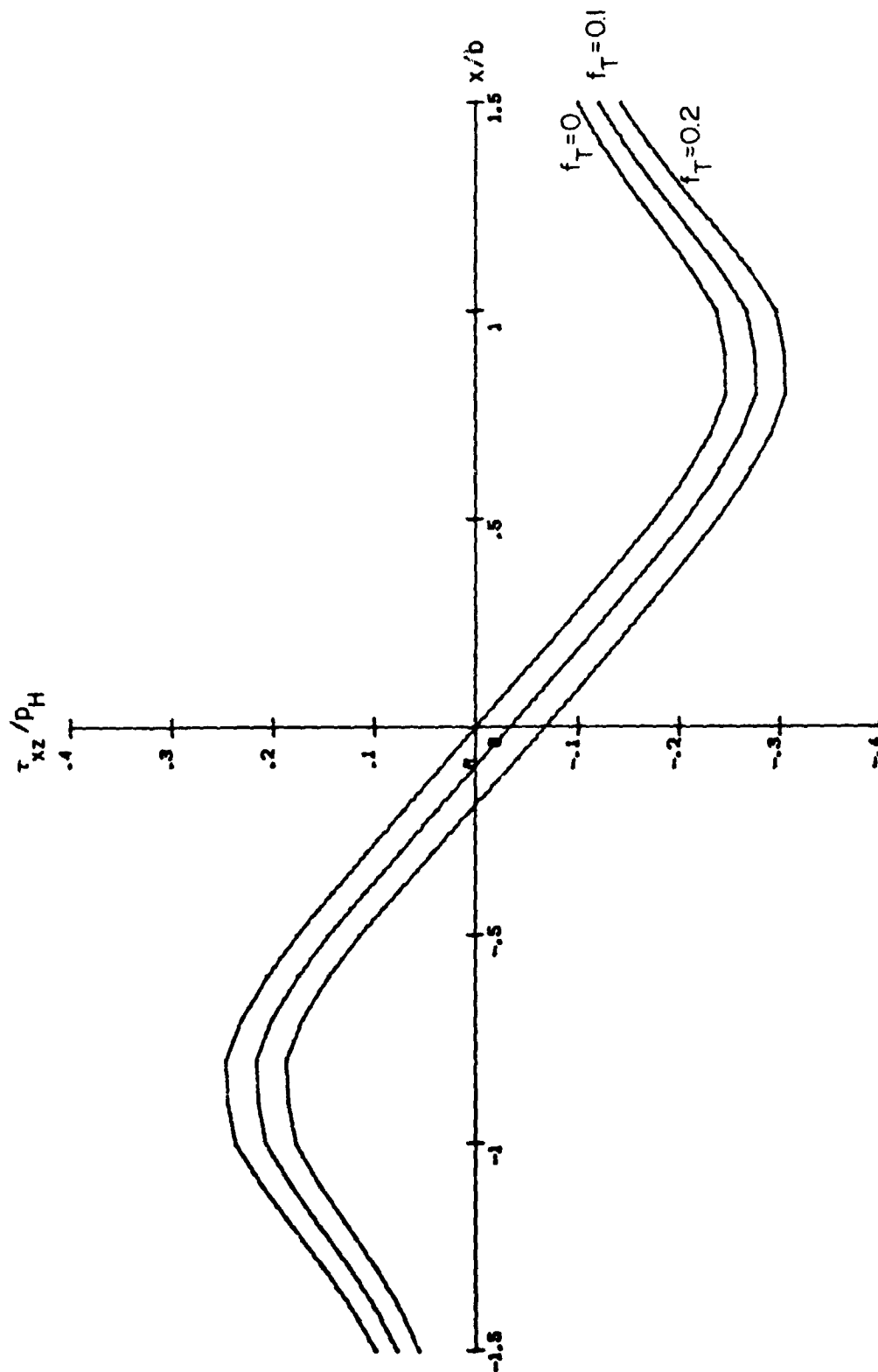


FIGURE 6. EFFECT OF FRICTION ON REVERSING ORTHOGONAL SHEAR STRESS
($K \approx 0$, $\nu = .285$, $z/b = .5$ T-Model)

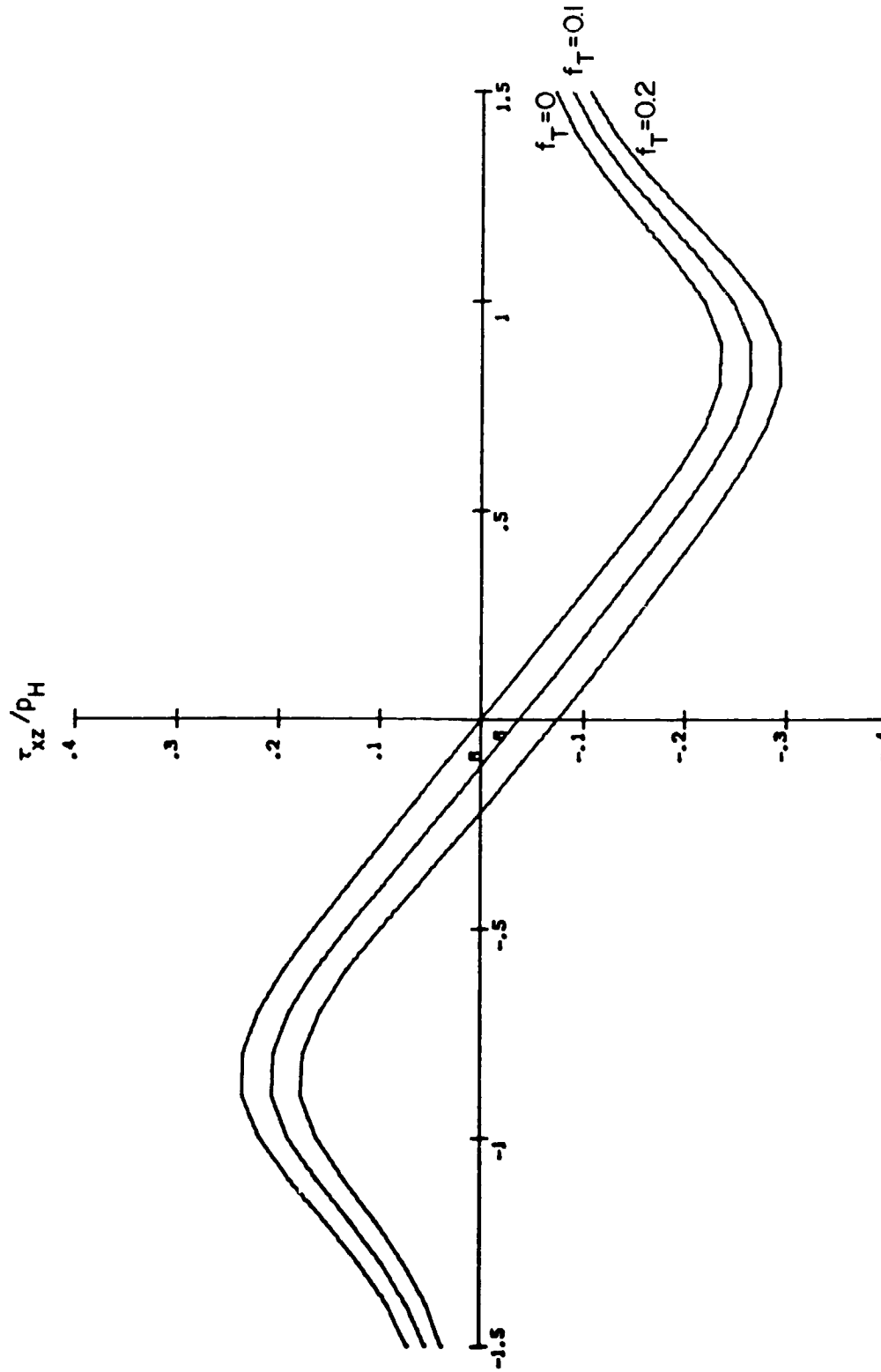


FIGURE 7. EFFECT OF FRICTION ON REVERSING ORTHOGONAL SHEAR STRESS
($K = .5$, $\nu = .285$, $z/b = .435$ T-Model)

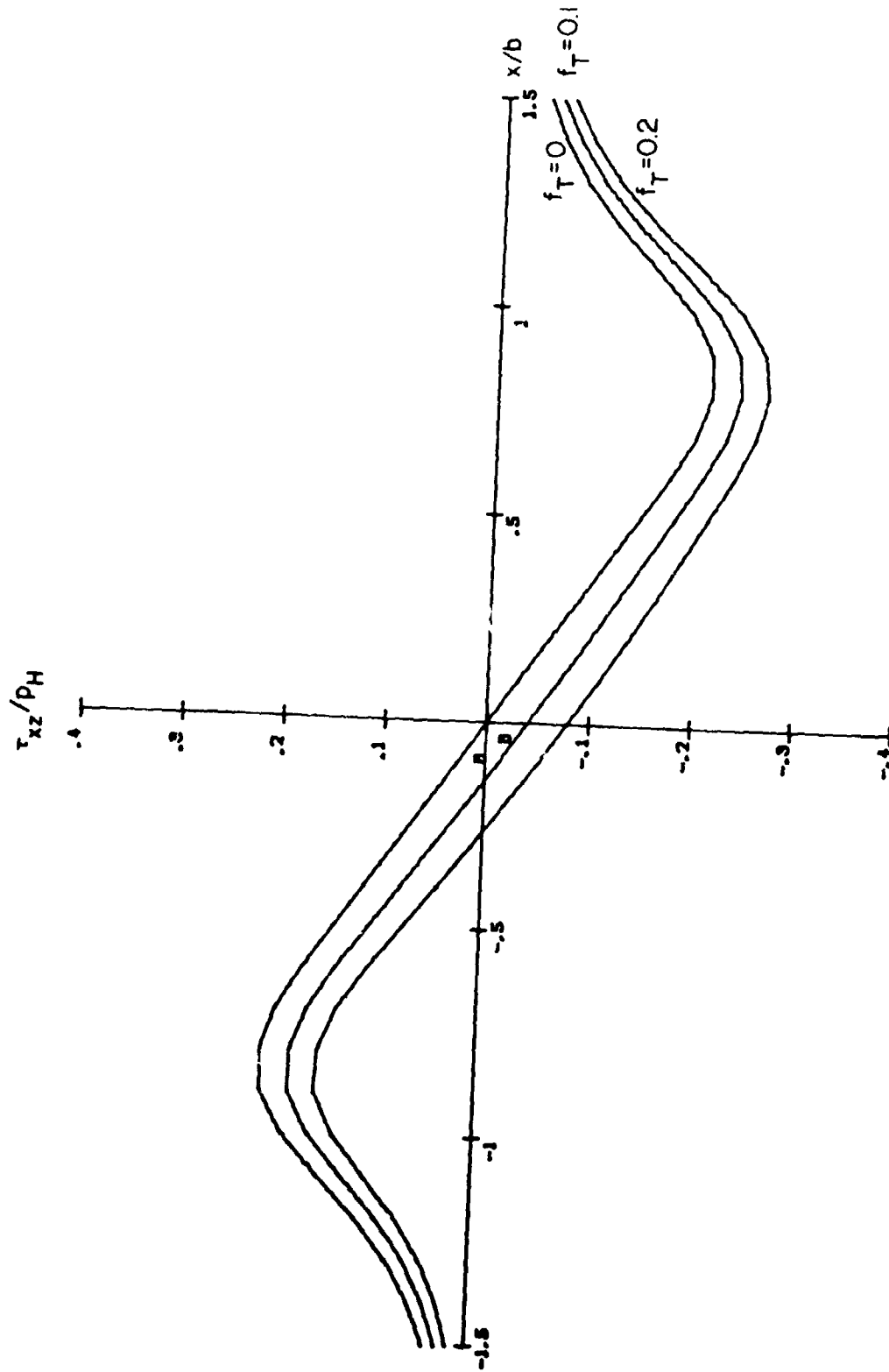


FIGURE 8. EFFECT OF FRICTION ON REVERSING ORTHOGONAL SHEAR STRESS
($K = 1$, $\nu = .285$, $z/b = .35$ T-Model)

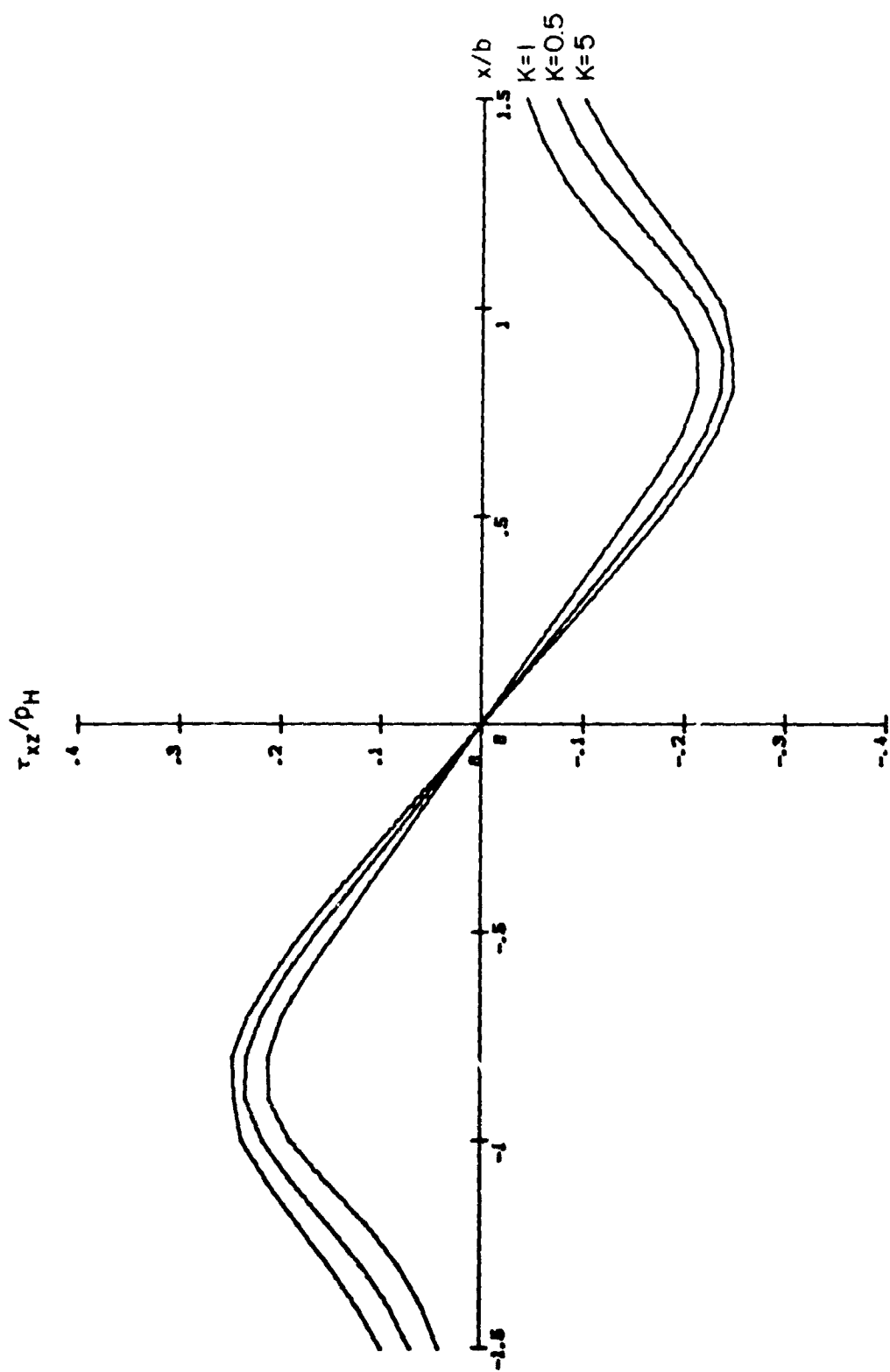


FIGURE 9. EFFECT OF ASPECT RATIO K ON REVERSING ORTHOGONAL SHEAR STRESS
 ($f_T = f_A = 0$, $\nu = .285$ T-Model)

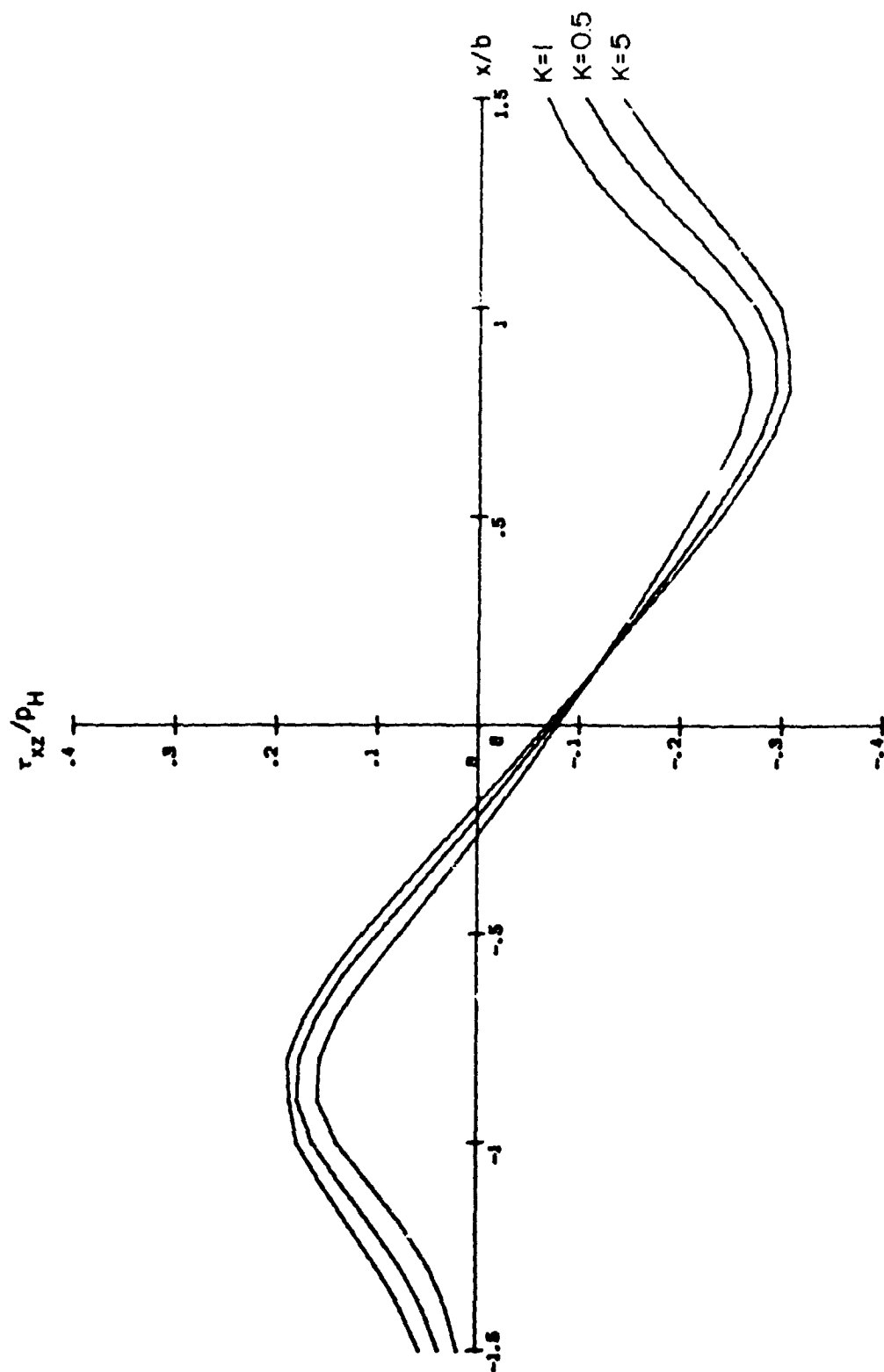


FIGURE 10. EFFECT OF ASPECT RATIO ON REVERSING ORTHOGONAL SHEAR STRESS
($f_v = .2$, $\nu = .285$ T-Model)

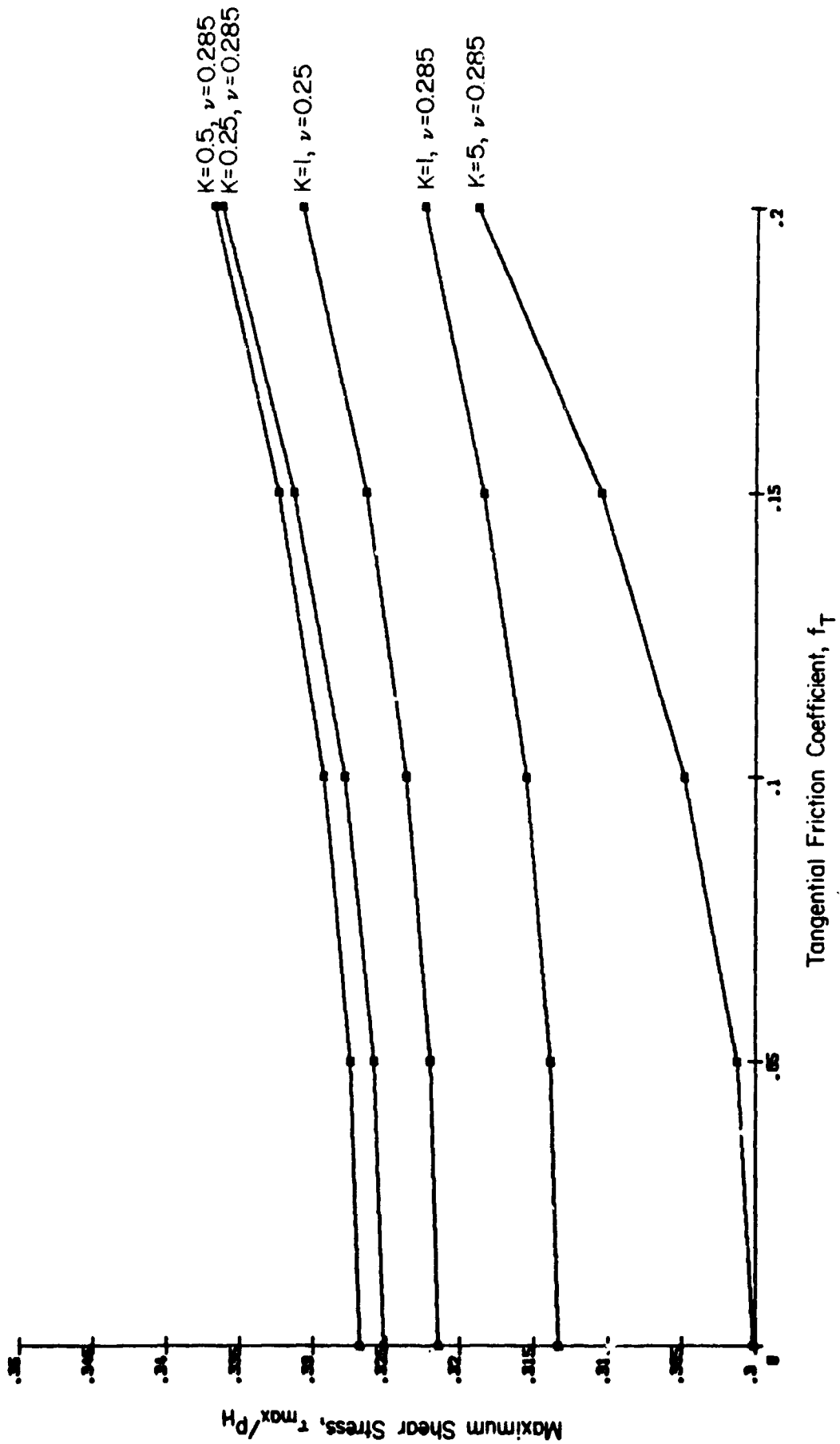


FIGURE 11. EFFECT OF FRICTION ON MAGNITUDE OF MAXIMUM SHEAR STRESS (T-Model)

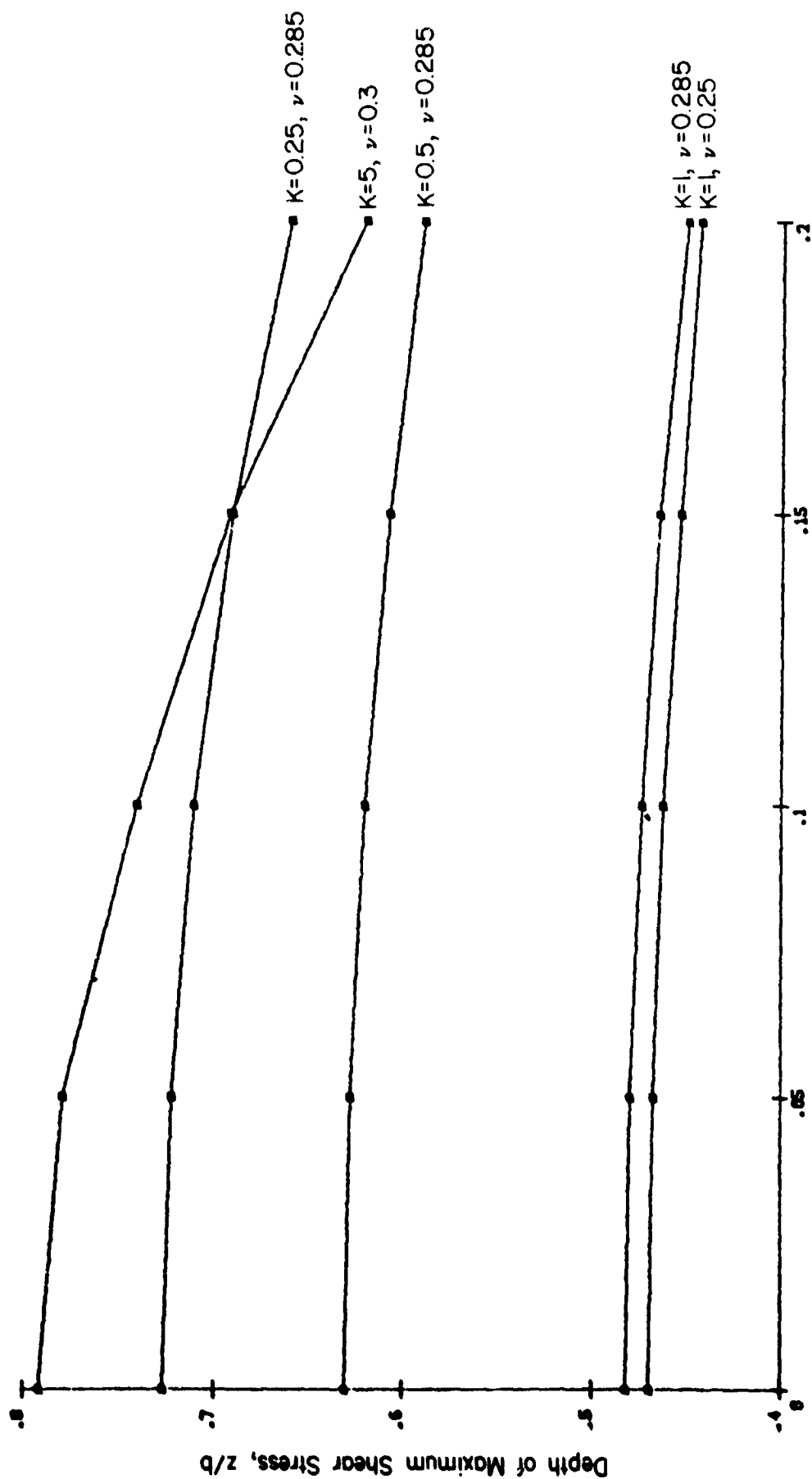


FIGURE 12. EFFECT OF FRICTION ON DEPTH OF MAXIMUM SHEAR STRESS
(T-model)

drives, only very small changes in stress depth and magnitude occur. Higher value of friction ($f = .2$) produces sizable increases in stress. The observations concerning shear stress also occur with regard to the octahedral shear stress as shown in Figures 13 and 14.

Figure 15 shows the effect of friction coefficient, f , on surface-shear-stresses-reversals for line ($K = 0$) contact. As can be observed, the magnitude of reversing stresses on the surface does not exceed the reversing orthogonal shear stress for values of $f < 0.25$. This implies that for this contact situation, fatigue-related stresses are not altered by friction for $f < 0.25$. Smith and Liu⁽⁵⁾ showed sizable effects at $f = 0.33$, which would be consistent with our computations. However, values of f of this magnitude should occur only in very poor lubrication situations and are not relevant to lubricated traction drive theory. As can be observed, friction does materially alter the shear stresses near the surfaces, even for low (< 0.1) friction coefficients. This implies that friction alters the overall stress field and could alter the propensity of the system to incur a surface or near surface initiated fatigue failure. Fatigue tests in conjunction with the stress model are badly needed to further extend our knowledge of the role of low levels of friction on fatigue.

Figure 16 shows a shear stress plot of τ_{xy} versus τ_{zx} for the plane of maximum shear stress at the center of contact very near the surface. The magnitude of the stress reversals envelope ($\approx .6$) is very consistent with the Smith-Liu⁽⁵⁾ computations and further illustrates the effect of severe friction ($f = .33$) on fatigue inducing stresses. However, the effect of friction on these stresses is not a factor at lower friction.

In conclusion, it can be said that based on the computer models discussed herein, low friction coefficient ($f < .1$) do not alter the fatigue stresses. At higher friction levels, changes will occur, but these cannot explain the observed effect of friction on fatigue. Other factors such as non-Hertzian pressures, thermal stress, and nonsymmetric tractions should then be included to understand the roll of friction on fatigue stress.

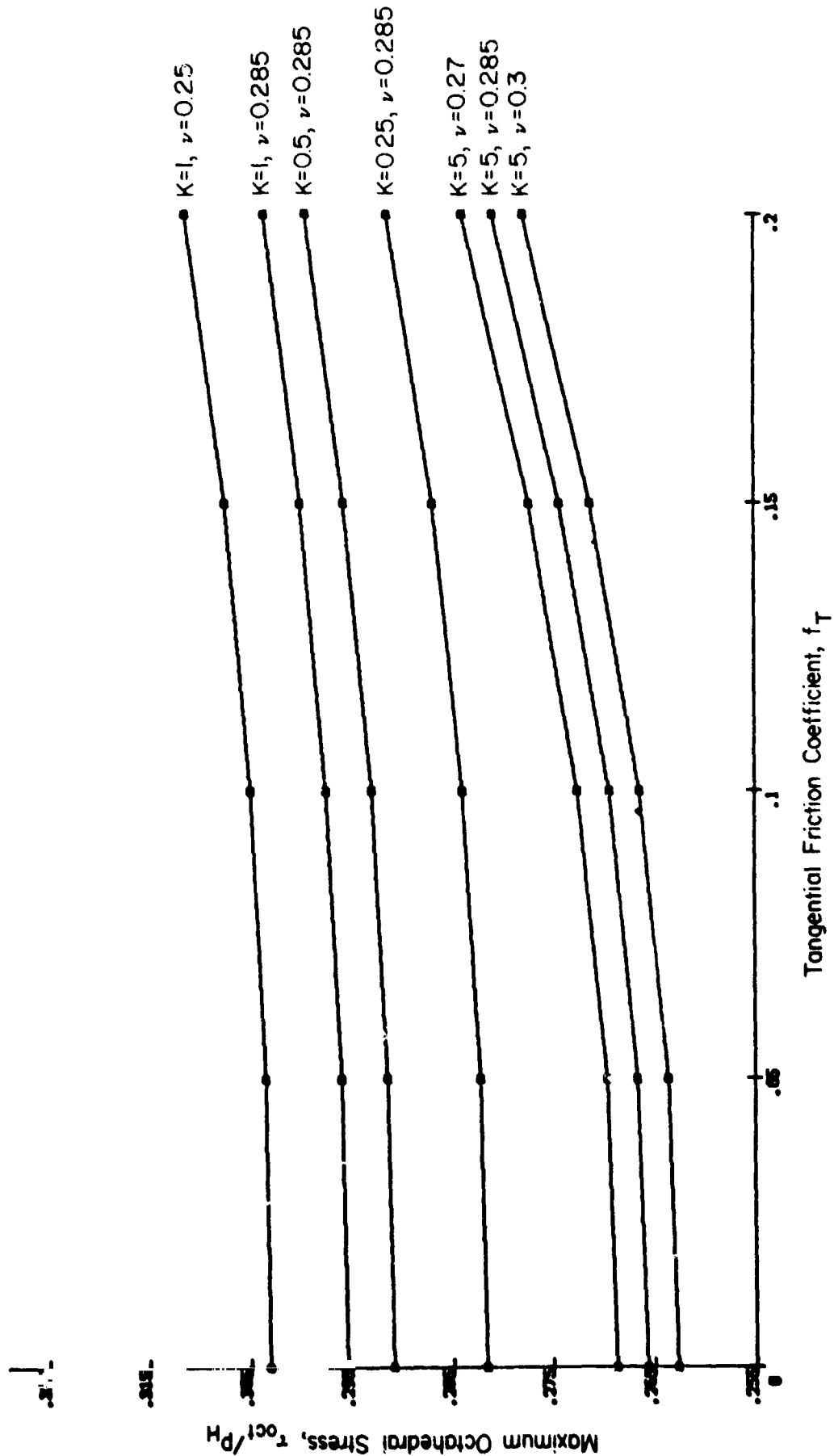


FIGURE 13. EFFECT OF FRICTION ON MAXIMUM OCTAHEDRAL SHEAR STRESS (T-Model)

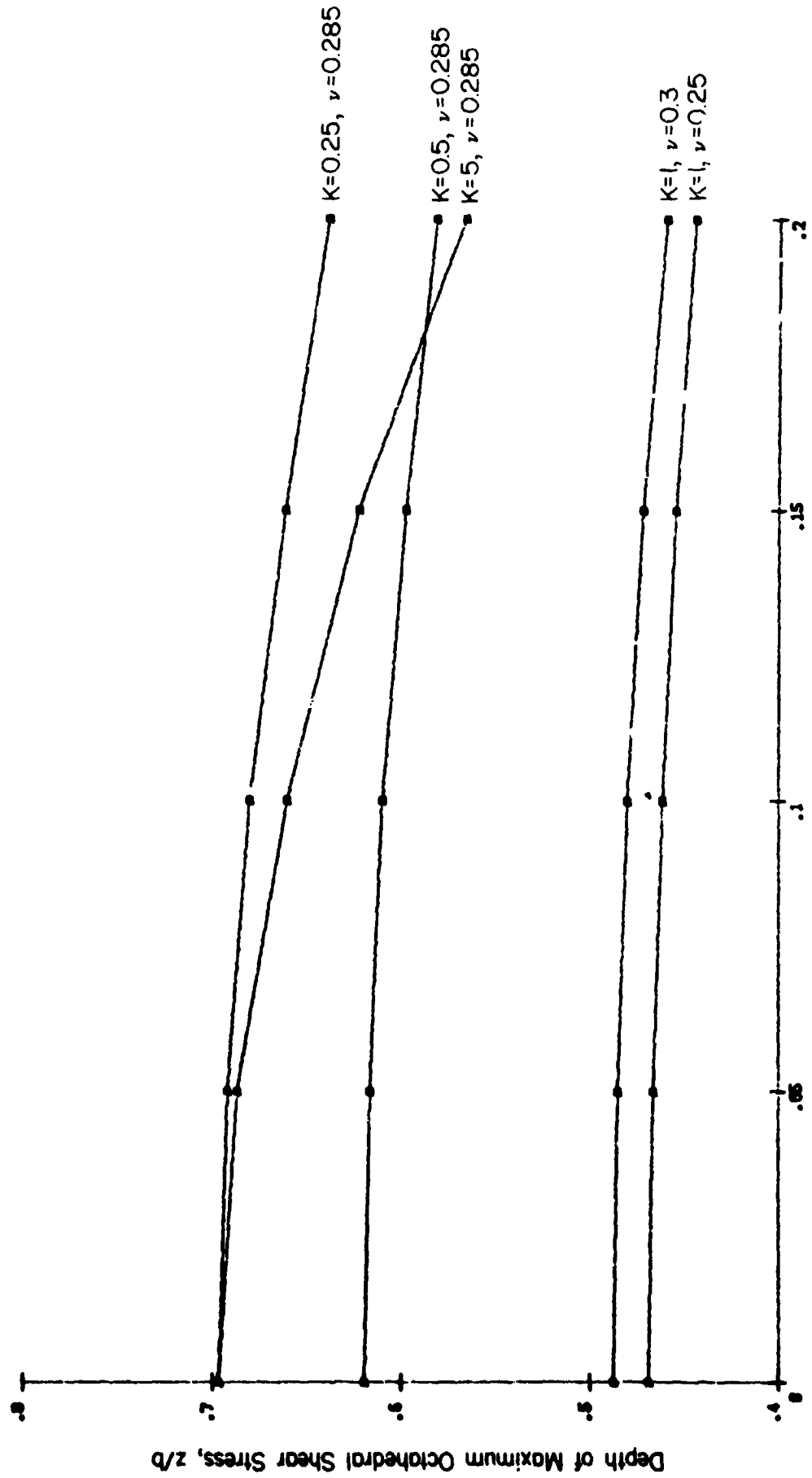


FIGURE 14. EFFECT OF FRICTION ON DEPTH OF MAXIMUM OCTAHEDRAL STRESS

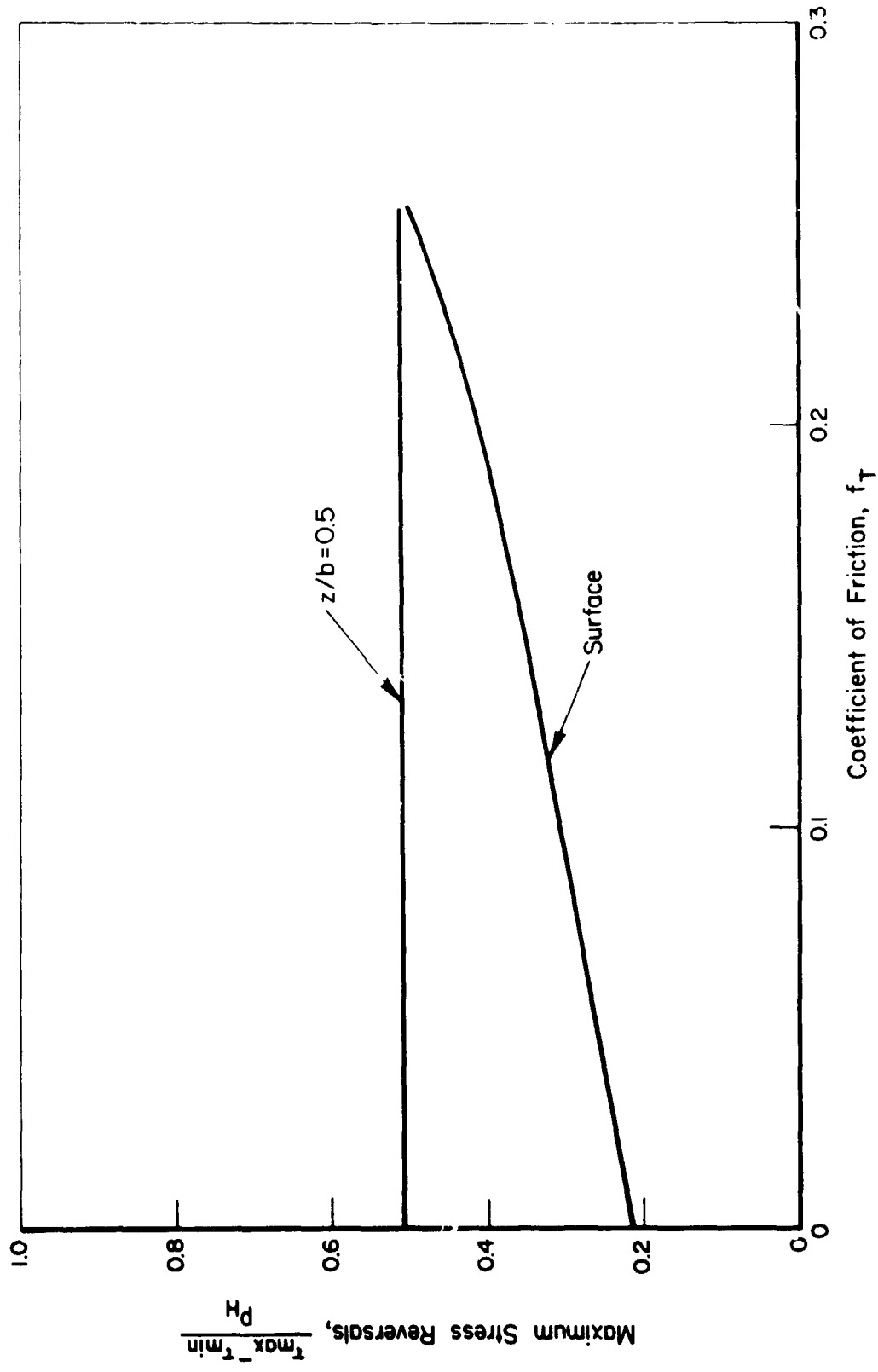


FIGURE 15. EFFECT OF FRICTION ON MAXIMUM STRESS REVERSALS
($K = 0$, $f_A = 0$, $\nu = .285$, B-Model)

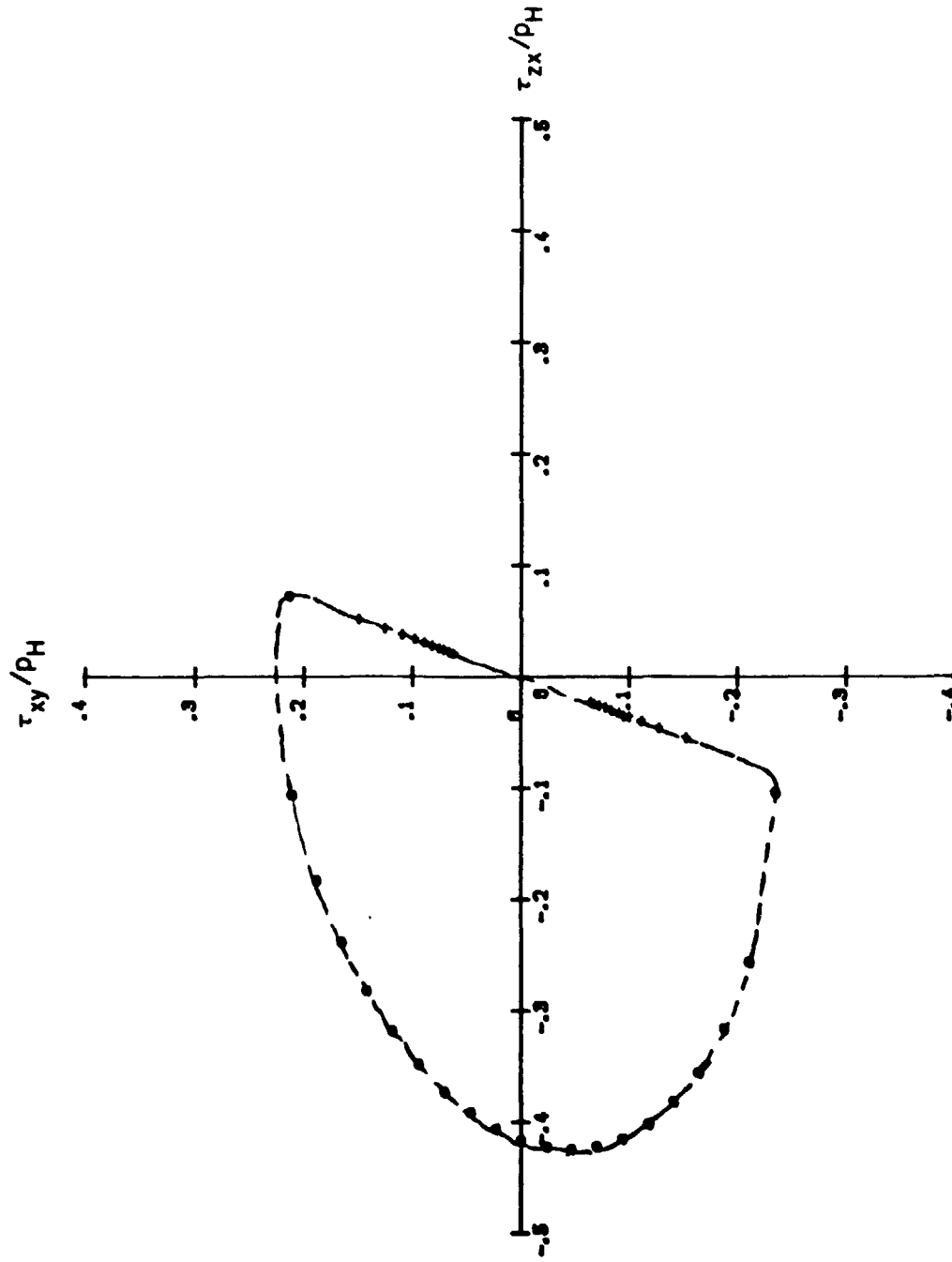


FIGURE 16. ILLUSTRATION OF VARIATION OF SHEAR STRESS ON PLANE OF MAXIMUM SHEARING STRESS
 ($z/b = 0$, $K = 0$, $\nu = .25$, $f_T = .333$ T-Model)

SUMMARY

The performance life of traction drives can be a very important factor in evaluating the overall effectiveness of the drive concept. Intuitively, this life should be heavily related to the state-of-stress in the elements as a result of high loads and tractions. The purpose of the project has been to develop a mathematical tool for evaluating this stress-state. Two independent, but similar, approaches (one at Battelle and one by Tevaarwerk) to developing the stress model have been pursued. Essentially, the models involve the computations of subsurface shear stresses (and stress reversals) as a result of normal and frictional loadings. Where possible the models have been checked against existing theory and against each other.

One use of the stress models has been to evaluate fatigue test methodology for a rolling contact (RC) fatigue tester. The standard RC tester consists of a small driven cylinder loaded between two larger crowned cylinders. The RC tester is a candidate device to evaluate the effect of traction on fatigue, either by driving the crowned rollers (tangential slip) or by simply skewing the rollers (axial slip); the skewing technique would be easier. The stress model was used to evaluate the effect of lubricated type tractions on stresses for a typical RC configuration.

The general conclusion from the RC evaluations was that the fatigue inducing stresses (shear stress) reversals and depth of shear stress are not seriously altered by tractions (axial or tangential) which are typical of lubricated contacts. There are some changes in the stress field, but these are difficult to relate to fatigue. To further explore the effect of friction on stress, additional computer cases have been evaluated.

The general conclusions from additional computer analyses is that friction coefficients of the order of 0.25 are required to materially alter the state of fatigue inducing stresses; this is much larger than would occur in lubricated contact. This implies then, that other effects not incorporated in the current stress-models should be included. These effects include non-Hertzian stresses distributions and thermal stresses. Both of these effects can impose nonsymmetrical (about the center of contact) shear stresses and thus will produce shear stress reversals which will superimpose on the normal and friction stresses.

REFERENCES

- (1) Lundberg, G. and Palmgren, A., "Dynamic Capacity of Rolling Bearings", Ing. Vetenskap, Akad.-Handl., No. 196, 1947.
- (2) Coy, J. J., Loewenthal, S.H., and Zaretsky, E.V., "Fatigue Life Analysis for Traction Drives with Applications to a Torodial-Type Geometry", NASA TND-8362.
- (3) Hertz, Heinrich, Miscellaneous Papers. Part V - The Contact of Elastic Solids, the MacMillan Company (London), pp 146-162, 1896.
- (4) Harris, Tedric A., Rolling Bearing Analysis, John Wiley & Sons, Inc., 1966.
- (5) Smith, T. O. and Liu, C. K., "Stresses Due to Tangential and Normal Loads on an Elastic Solid with Application to Some Contact Stress Problems", Trans. ASME, J.O.A.M., pp 157-166, June 1953.
- (6) Hamilton, G. M. and Goodman, L. E., "The Stress Field Created by a Circular Sliding Contact", Trans. ASME, J.O.A.M., 33, E, pp 371-376, 1966.
- (7) Kuznetsov, Ye. A., "The Superposition Principle in the Solution of Contact Friction Stress Problems", Wear, 50, pp 183-189, 1978.
- (8) Shames, I. H., Mechanics of Deformable Solids, Prentice Hall, Englewood Cliffs, N.J., pp 15-29, 1964.
- (9) Mindlin, R. D., "Force at a Point in the Interior of a Semi-Infinite Solid", Physics, Vol. 7, pp 195-202, May 1936.

APPENDIX A

COMPUTATIONS OF THE STRESS TENSOR

APPENDIX A

COMPUTATIONS OF THE STRESS TENSORStress Due to Point Loads

The state of stress at any point on or beneath the surface of a system under concentrated contact is quite complex. To define this stress state at each point requires the computations of nine components of the stress tensor as related to contact pressures and tractions. The effect of pressures and tractions on stress were developed by Mindlin⁽⁹⁾ for point loadings on the surface of a semiinfinite body using the coordinate system of Figure A-1, and letting $R^2 = x^2 + y^2 + z^2$. These equations appear as follows.

Normal Load.

$$\sigma'_{xN} = \frac{P_N}{2\pi} \left\{ \frac{(1-2\nu)z}{R^3} - \frac{3x^2z}{R^5} - \frac{(1-2\nu)}{R(R+z)} \left[1 - \frac{x^2}{R(R+z)} - \frac{x^2}{R^2} \right] \right\}, \quad (A-1)$$

$$\sigma'_{yN} = \frac{P_N}{2\pi} \left\{ \frac{(1-2\nu)z}{R^3} - \frac{3y^2z}{R^5} - \frac{(1-2\nu)}{R(R+z)} \left[1 - \frac{y^2}{R(R+z)} - \frac{y^2}{R^2} \right] \right\}, \quad (A-2)$$

$$\sigma'_{zN} = -\frac{3P_N z^3}{2\pi R^5}, \quad (A-3)$$

$$\tau'_{zyN} = \tau'_{yzN} = -\frac{3P_N y z^3}{2\pi R^5}, \quad (A-4)$$

$$\tau'_{xz_N} = \tau'_{zx_N} = -\frac{3}{2\pi} \frac{P_N x z^2}{R^5}, \quad (A-5)$$

$$\tau'_{yx_N} = \tau'_{xy_N} = \frac{P_N xy}{2\pi} - \frac{3z}{R^5} + \frac{(1-2\nu)(2R+z)}{R^3(R+z)^2}. \quad (A-6)$$

Tangential Load.

$$\sigma'_{x_T} = \frac{P_T x}{2\pi} \left[\frac{1-2\nu}{R^3} - \frac{3x^2}{R^5} - \frac{(1-2\nu)}{R(R+z)^2} \right] - \frac{x^2(3R+z)}{R^2(R+z)}, \quad (A-7)$$

$$\sigma'_{y_T} = \frac{P_T x}{2\pi} \left[\frac{1-2\nu}{R^3} - \frac{3y^2}{R^5} - \frac{(1-2\nu)}{R(R+z)^2} \right] - \frac{y^2(3R+z)}{R^2(R+z)}, \quad (A-8)$$

$$\sigma'_{z_T} = -\frac{3P_T x z^2}{2\pi R^5}, \quad (A-9)$$

$$\tau'_{zy_T} = \tau'_{yz_T} = -\frac{3P_T xyz}{2\pi R^5}, \quad (A-10)$$

$$\tau'_{xz_T} = \tau'_{zx_T} = -\frac{3P_T x^2 z}{2\pi R^5}, \quad (A-11)$$

$$\tau'_{yx_T} = \tau'_{xy_T} = \frac{P_T y}{2\pi} \left[\frac{1-2\nu}{R^3} - \frac{3x^2}{R^5} - \frac{(1-2\nu)}{R(R+z)^2} \right] - \frac{x^2(3R+z)}{R^2(R+z)}. \quad (A-12)$$

Axial Load.

$$\sigma'_{x_A} = \frac{P_A y}{2\pi} \left[\frac{1-2\nu}{R^3} - \frac{3x^2}{R^5} - \frac{(1-2\nu)}{R(R+z)^2} \right] - \frac{x^2(3R+z)}{R^2(R+z)}, \quad (A-13)$$

$$\sigma'_{y_A} = \frac{P_A y}{2\pi} \left\{ \frac{1-2\nu}{R^3} - \frac{3y^2}{R^5} - \frac{(1-2\nu)}{R(R+z)^2} \left[3 - \frac{y^2(3R+z)}{R^2(R+z)} \right] \right\}, \quad (A-14)$$

$$\sigma'_{z_A} = -\frac{3 P_A y z^2}{2\pi R^5}, \quad (A-15)$$

$$\tau'_{zx_A} = \tau'_{xz_A} = -\frac{3 P_A x y z}{2\pi R^5}, \quad (A-16)$$

$$\tau'_{zy_A} = \tau'_{yz_A} = -\frac{3 P_A y^2 z}{2\pi R^5}, \quad (A-17)$$

$$\tau'_{xy_A} = \tau'_{yx_A} = \frac{P_A x}{2\pi} \left\{ -\frac{3y^2}{R^5} - \frac{(1-2\nu)}{R(R+z)^2} \left[1 - \frac{y^2(3R+z)}{R^2(R+z)} \right] \right\}. \quad (A-18)$$

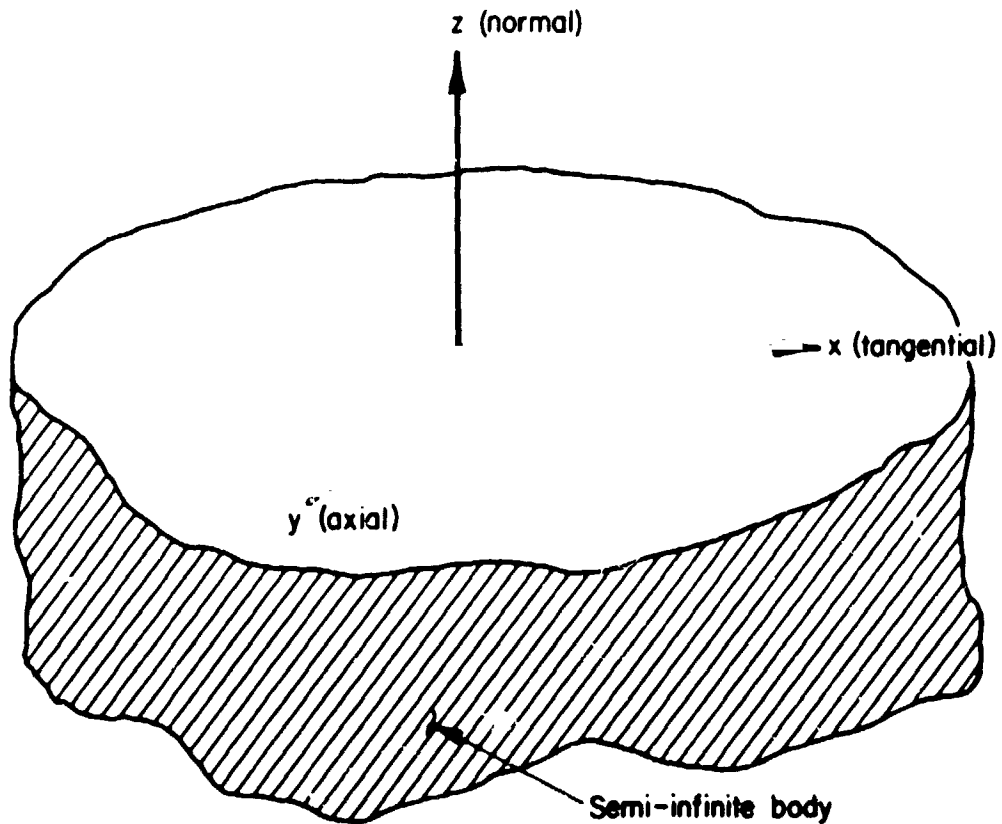


FIGURE A-1. COORDINATE SYSTEM FOR STRESS COMPUTATIONS

Hertzian Pressures and Surface Traction

For a point on the surface, the normal load could be written

$$P_N = p dx dy \quad \text{where } p \text{ is the local pressure} \quad (A-19)$$

Also, $P_T = p f_T dx dy$ and (A-20)

$$P_A = p f_A dx dy \quad (A-21)$$

where f_T and f_A are the effective coefficients of friction acting tangential or axially to the surface.

If the surface were subjected to a Hertzian pressure distribution, the pressure could be expressed (see Figure A-2):

$$p = p_H \sqrt{1 - \frac{(x - x_1)^2}{b^2} - \frac{(y - y_1)^2}{a^2}}, \quad (A-22)$$

where p_H is the maximum Hertz pressure, a and b are the major and minor axes of the contact ellipse, x and y are the coordinates with origins at the center of the ellipse and x_1 and y_1 are locations of the point load relative to the center of the Hertz ellipse. The Battelle analyses were restricted to the case where $y_1 = 0$. Tevaarwerk allowed y_1 to be a variable and found $y_1 = 0$ to be the interesting region.

The general approach for determining the nine components of the stress tensor at any point can be written

$$\sigma_{ij} = p_H \iint_A \left[\frac{\sigma'_{ijN}}{P_N} + \frac{f_T \sigma'_{ijT}}{P_T} + \frac{f_A \sigma'_{ijA}}{P_A} \right] \sqrt{1 - \frac{(x - x_1)^2}{b^2} - \frac{y^2}{a^2}} dx dy, \quad (A-23)$$

where σ_{ij} represents nine components of the stress tensor* for Hertzian pressures and various frictional forces and σ'_{ij} are the results of Mindlin's analyses (discussed in the previous section). In further computations, we

* In tensor notation σ_{ij} implies $\sigma_{11}, \sigma_{12}, \sigma_{13}, \sigma_{21}, \dots, \sigma_{33}$, where σ_{11} is σ_x , σ_{12} is τ_{xy} , σ_{22} is σ_y , σ_{23} is τ_{yz} , etc.

shall use $\bar{\sigma}_{ij} = \sigma_{ij}/p_H$ such that all computations will be normalized on the Hertz maximum pressures.

It would serve no purpose to show all substitutions of Mindlin's equations into the general stress tensor equation. It can be noted that any of Mindlin's equations containing the term y^n (n odd) will produce a zero integral since the integration involves that function times the even Hertz pressure over the whole pressure region for $y_1 = 0$. As an example of how the substitution occurs, consider the normal stress $\bar{\sigma}_z$ for f_T and $f_A = 0$.

$$\bar{\sigma}_z \equiv \bar{\sigma}_{33} = \int_{-a}^a \int_L^U \frac{3}{2\pi} \frac{z^3}{R^5} \sqrt{1 - \left(\frac{x - x_1}{b}\right)^2 - \frac{y^2}{a^2}} \, dx dy, \quad (A-24)$$

where the lower limit $L = x_1 - b \sqrt{1 - \frac{y^2}{a^2}}$, and

the upper limit $U = x_1 + b \sqrt{1 - \frac{y^2}{a^2}}$.

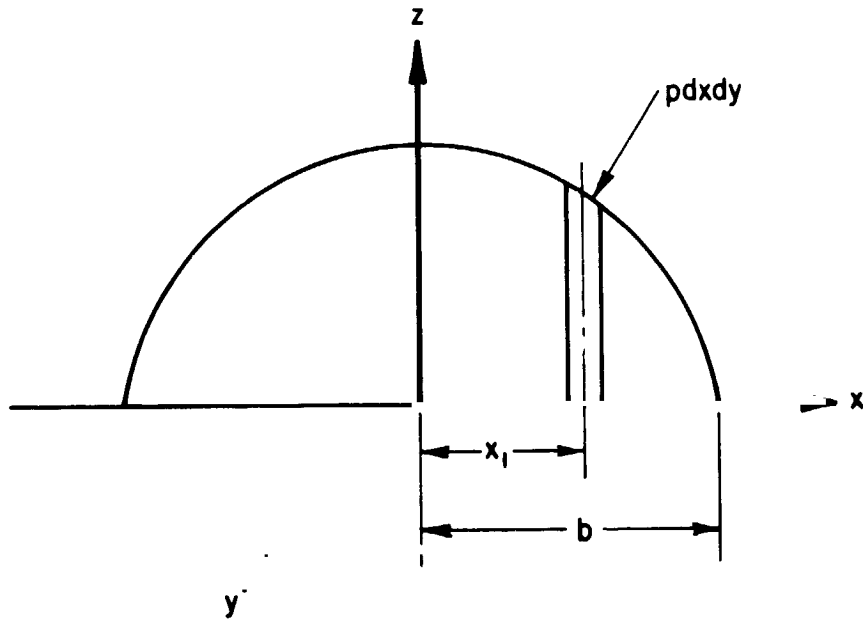


FIGURE A-2. LOADING CHARACTERIZED BY HERTZIAN ELLIPSE

Scaling the Stress Tensor Equations

The following substitutions were used to facilitate computations:

$$\bar{z} = z/b \quad \xi = x/z \quad \eta = y/z \quad K = b/a \quad \text{and} \quad \bar{x}_1 = x_1/b \quad .$$

With these substitutions Equation A-24 appears

$$\bar{\sigma}_z = \frac{3}{2\pi} \int_{-1/K\bar{z}}^{1/K\bar{z}} \int_{\bar{L}}^{\bar{U}} \frac{1}{\bar{R}^5} \sqrt{1 - (\bar{z}\xi - \bar{x}_1)^2 - (K\bar{z}\eta)^2} \, d\xi d\eta \quad , \quad (\text{A-25})$$

where

$$\bar{L} = \bar{x}_1/\bar{z} - 1/\bar{z} \sqrt{1 - (\bar{z}K\eta)^2} \quad ,$$

$$\bar{U} = \bar{x}_1/\bar{z} + 1/\bar{z} \sqrt{1 - (\bar{z}K\eta)^2} \quad , \text{ and}$$

$$\bar{R} = \sqrt{\xi^2 + \eta^2 + 1} \quad .$$

This type of substitution permitted reasonable computations near $\bar{z} = 0$.

In the computer solution

$$\bar{\sigma}_z = \frac{3}{2\pi} \quad (2) \int_0^\infty \int_{-\infty}^\infty \frac{\sqrt{A}}{\bar{R}^5} \, d\xi d\eta \quad , \quad (\text{A-26})$$

where

$$A = \begin{cases} 1 - (\bar{z}\xi - \bar{x}_1)^2 - (K\bar{z}\eta)^2 & (\text{A positive}) \\ 0 & (\text{otherwise}) \end{cases} \quad .$$

All other stress components were treated in the same manner using the general expression

$$\bar{\sigma}_{ij} = 2 \int_0^{\infty} \int_{-\infty}^{\infty} \left[\frac{\bar{\sigma}'_{ijN}}{P_N} + \frac{f_T \bar{\sigma}'_{ijT}}{P_T} + \frac{f_A \bar{\sigma}'_{ijA}}{P_A} \right] \sqrt{A} \, d\xi \, d\eta, \quad (A-27)$$

where by substituting $\xi = x$, $\eta = y$ and $z = 1$, all equations for σ'_{ij} become the equations for $\bar{\sigma}'_{ij}$.

Review

This is the most involved section in the report and may be difficult for the reader to readily grasp. Basically, all it involves is to take Mindlin's equations (A-1 - A-18), replace x with ξ , y with η , and z with 1 and integrate equation A-27. For example, suppose we want to calculate $\bar{\sigma}_{13} = \tau_{xz}$ from the normal load equation

$$\frac{\bar{\sigma}'_{13N}}{P_N} = - \frac{3}{2\pi} \frac{\xi}{R^5} \quad (\text{Equation A-5}) \quad (A-28)$$

From the tangential load equation

$$\frac{\bar{\sigma}'_{13T}}{P_T} = - \frac{3}{2\pi} \frac{\xi^2}{R^5} \quad (\text{Equation A-11}) \quad (A-29)$$

From the axial load equation

$$\frac{\bar{\sigma}'_{13A}}{P_A} = - \frac{3}{2\pi} \frac{\xi\eta}{R^5} \quad (\text{Equation A-16}), \quad (A-30)$$

where $\bar{R} = \sqrt{1 + \xi^2 + \eta^2}$.

Equation A-27 then becomes

$$\sigma_{13} = -2 \int_0^{\infty} \int_{-\infty}^{\infty} \frac{3 \bar{R}^5}{2\pi} \left[\xi + \xi^2 + \xi \eta \right] \sqrt{A} \, d\xi \, d\eta \quad . \quad (A-31)$$

This equation can be solved by numerical computation. In the Battelle computations, the integral on ξ was performed by a Gaussian quadrature approach and the η integration was performed by a Trapezoidal rule.

Check of Numerical Solution

Hamilton and Goodman⁽⁶⁾ developed an exact solution for circular contacts ($K = 1$). The numerical solution is compared with the exact solution in Table A-1; the exact solution was generated as a part of the work of Tevaarwerk. The agreement tends to verify the numerical accuracy.

Smith & Liu⁽⁵⁾ developed an exact solution for line contact ($K = 0$). The numerical solution is compared with the exact solution in Table A-2.

TABLE A-1. COMPARISON OF NUMERICAL SOLUTION WITH EXACT SOLUTION FOR $K = 1$ (6)
 $(\nu = 0.3, f_T = f_A = 0)$

x/b	z/b	σ_x		σ_y		σ_z		τ_{xy}		τ_{yz}		τ_{xz}	
		Num	Exact	Num	Exact	Num	Exact	Num	Exact	Num	Exact	Num	Exact
.1	-.8	-.305	-.300	-.361	-.356	-.579	-.573	0	0	0	0	.121	.119
	-.5	-.507	-.501	-.532	-.524	-.862	-.853	0	0	0	0	.057	.056
	-.3	-.581	-.575	-.591	-.583	-.953	-.943	0	0	0	0	.031	.031
	0	-.620	-.614	-.623	-.614	-1.00	-.99	0	0	0	0	0	0
	.3	-.581	-.575	-.591	-.583	-.953	-.943	0	0	0	0	-.031	-.031
	.5	-.507	-.501	-.532	-.524	-.861	-.853	0	0	0	0	-.057	-.056
.4	.8	-.305	-.300	-.360	-.356	-.579	-.573	0	0	0	0	-.121	-.119
	-.8	-.184	-.184	-.128	-.129	-.450	-.445	0	0	0	0	.213	.212
	-.5	-.212	-.212	-.198	-.199	-.717	-.709	0	0	0	0	.150	.149
	-.3	-.235	-.235	-.230	-.231	-.818	-.809	0	0	0	0	.090	.090
	0	-.252	-.250	-.249	-.250	-.871	-.862	0	0	0	0	0	0
	.3	-.235	-.235	-.230	-.231	-.817	-.809	0	0	0	0	-.090	-.090
.5	.5	-.212	-.212	-.198	-.199	-.717	-.709	0	0	0	0	-.150	-.149
	.8	-.185	-.184	-.128	-.129	-.450	-.445	0	0	0	0	-.213	-.212

TABLE A-2. COMPARISON OF NUMERICAL SOLUTION WITH EXACT SOLUTION FOR $K = 0$ ⁽⁵⁾
 $(\nu = .285, f_A = 0)$

f_T	z/b	x/b	σ_x		σ_y		σ_z		τ_{xy}		τ_{yz}		τ_{yz}	
			Num	Exact	Num	Exact	Num	Exact	Num	Exact	Num	Exact	Num	Exact
0	.5	-.8	-.298	-.299	-.240	-.227	-.506	-.500	0	0	0	0	.249	.247
		-.5	-.311	-.313	-.314	-.301	-.751	-.745	0	0	0	0	.180	.176
		-.3	-.328	-.329	-.346	-.334	-.850	-.842	0	0	0	0	.109	.107
		0	-.342	-.342	-.367	-.352	-.905	-.894	0	0	0	0	0	0
		.3	-.328	-.329	-.346	-.334	-.850	-.842	0	0	0	0	-.109	-.107
		.5	-.311	-.313	-.314	-.301	-.751	-.745	0	0	0	0	-.180	-.176
.15	.5	.8	-.298	-.299	-.240	-.227	-.506	-.500	0	0	0	0	-.249	-.247
		-.8	-.228	-.229	-.209	-.200	-.468	-.462	0	0	0	0	.203	.202
		-.5	-.259	-.263	-.290	-.280	-.724	-.718	0	0	0	0	.133	.129
		-.3	-.295	-.297	-.331	-.320	-.834	-.826	0	0	0	0	.059	.057
		0	-.342	-.342	-.367	-.353	-.905	-.894	0	0	0	0	-.052	-.051
		.3	-.361	-.362	-.360	-.348	-.867	-.858	0	0	0	0	-.159	-.157
.15	.5	.5	-.363	-.364	-.337	-.324	-.779	-.771	0	0	0	0	-.227	-.222
		.8	-.369	-.369	-.272	-.260	-.543	-.536	0	0	0	0	-.295	-.292

APPENDIX B

SOURCE LISTING FOR
BATTELLE STRESS MODEL

	PROGRAM SUBSTS(INPUT,OUTPUT,TAPE 1)	000100
	COMMON/F/ ISTRSS,X1(22,1),GNU,Z,Y,XK,FT,FA,MX	000110
	COMMON/C/ STRSS(3,3,22)	000120
	DIMENSION AN(3,3),ASM(3,22),AS(3,22),BN1(3),BN2(3)	000130
	1,CN1(3,22),CN2(3,22),CN3(3,22)	000140
	REWIND 1	000150
	BN1(1)=.70711	000160
	BN1(2)=0.	000170
	BN1(3)=-.70711	000180
	BN2(1)=.57735	000190
	BN2(2)=.57735	000200
	BN2(3)=.57735	000210
	CN3(1,1)=0.	000220
	CN3(2,1)=0.	000230
	CN3(3,1)=1.	000240
	SIGN=+1.	000250
	SIGNA=+1.	000260
8	PRINT 6	000270
6	FORMAT(* INPUT,ASPECT RATIO,NU,Z,FT,FA,X-POSS,CASE-NO*)	000280
	READ*,XK,GNU,Z,FT,FA,MX,NCASE	000290
	IF(XK.LT.0.) GO TO 7	000300
	WRITE(1,13) NCASE	000310
13	FORMAT(///,50X,* CASE NUMBER=*,I8,///)	000320
	WRITE(1,9) XK,GNU,Z,FT,FA	000330
	PRINT 9,XK,GNU,Z,FT,FA	000340
9	FORMAT(* K=*,E12.5, * NU=*,E12.5, * Z=*,E12.5, * FT=*,E12.5, * FA=*,	000350
	E12.5,///)	000360
	TMXXM=TMXXQ=TAURVM=TAURVQ=0.	000370
	IF(XK.LT.1.E-6) CALL STRSSC(1)	000380
	IF(XK.GT.1.E-6) CALL STRSSC(6)	000390
	WRITE(1,12)	000400
12	FORMAT(* IX SXZ SXX S1 SY S2 SZZ S3 SXY	000410
	1SYZ SXZ SXX S1 S2 S3 X-POS	000420
	1*///)	000430
	DO 1 IX=1,MX	000440
	CALL PRINC(ISTRSS,IX,S1,S2,S3)	000450
	CALL ANGLP(ISTRSS,S1,S2,S3,AN,IX,SIGNA)	000460
	CALL ANGTRAN(AN,BN1,CN1,IX)	000470
	CALL ANGTRAN(AN,BN2,CN2,IX)	000480
	WRITE(1,11) IX,STRSS(1,1,IX),STRSS(2,2,IX),STRSS(3,3,IX),	000490
	1STRSS(1,2,IX),STRSS(2,3,IX),STRSS(1,3,IX),S1,S2,S3,X1(IX,1)	000500
11	FORMAT(I5,10E12.5)	000510
1	CONTINUE	000520
	WRITE(1,20)	000530
20	FORMAT(//,45X,* FATIGUE SHEAR STRESS SUMMARY * ///	000540
	DO 21 IXRF=1,MX	000550
	IXRF=X1(IXRF,1)	000560
	CALL RVSTRS(ISTRSS,CN1,ASM,TRVM,TMAX,IXRF,SIGN)	000570
	PRINT 99,TMAX	000580
99	FORMAT(* TMAX=*,E12.5)	000590
	IF(ABS(TRVM).GT.ABS(TAURVM)) TAURVM=TRVM	000600
	IF(ABS(TMAX).GT.ABS(TMXXM)) 22,23	000610
22	TMXXM=TMAX	000620
	IXRFM=IXRF	000630
	SIGN=-1.	000640
23	CALL RVSTRS(ISTRSS,CN2,AS,TRVMO,TMAXO,IXRF,SIGN)	000650
	IF(ABS(TRVMO).GT.ABS(TAURVO)) TAURVO=TRVMO	000660
	IF(ABS(TMAXO).GT.ABS(TMXXO)) 24,25	000670
24	TMXXO=TMAXO	000680
	IXRFO=IXRF	000690
25	CONTINUE	000700
	PRINT 29,IXRF,TRVM,TMAX,TRVMO,TMXXO	000710
29	FORMAT(I5,4E14.5)	000720

21	CONTINUE	000730
	WRITE(1,15)	000740
15	FORMAT(//,20X,* PLANE OF MAX SHEAR STRESS*//)	000750
	WRITE(1,18) TMXXM,CN1(1,IXRFM),CN1(2,IXRFM),CN1(3,IXRFM),X1(IXRFM,	000760
	1,E13.5,* X-REF=*,E13.5)	000790
	WRITE(1,19) TAURVM,ASM(1,IXRFM),ASM(2,IXRFM),ASM(3,IXRFM)	000800
19	FORMAT(* TAU REVERSING=*,E13.5,* AS(1)=*,E13.5,* AS(2)=*,E13.5,	000810
	1*AS(3)=*,E13.5)	000820
	WRITE(1,16)	000830
16	FORMAT(//,20X,* PLANE OF MAX OCT SHEAR STRESS *//)	000840
	WRITE(1,19) TMXXO,CN2(1,IXRFO),CN2(2,IXRFO),CN2(3,IXRFO),X1(IXRFO,	000850
	11)	000860
	WRITE(1,19) TAURVO,AS(1,IXRFO),AS(2,IXRFO),AS(3,IXRFO)	000870
	CALL RVSTRS(STRSS,CN3,AS,TRVM,TMAX,1,SIGN)	000880
	WRITE(1,17)	000890
17	FORMAT(//,20X,* PLANE OF REVERSING SHEAR STRESS *//)	000900
	WRITE(1,18) TMAX,CN3(1,1),CN3(2,1),CN3(3,1)	000910
	WRITE(1,19) TRVM,AS(1,1),AS(2,1),AS(3,1)	000920
	WRITE(1,20)	000930
20	FORMAT(141)	000940
	GO TO 8	000950
7	CONTINUE	000960
	END	000970
	SUBROUTINE STRSSC(IFLAG)	000980
	COMMON/F/ IS,X1(22,1),GNU,Z,Y,XK,FT,FA,MX1	000990
	COMMON/C/ STRSS(3,3,22)	001000
	DIMENSION FI(22,17),GINT(22),ICALC(22),TEMP1(22),FX(22),FIY(17)	001010
	1,Y1(17)	001020
	PI=3.14159	001030
	MY=17	001040
	MX=MX1	001050
	CALL XPOS	001060
	IF(IFLAG.EQ.1) GO TO 10	001070
	DO 9 ISTRSS=1,6	001080
	IS=ISTRSS	001090
	DO 4 JY=1,MY	001100
	IF(JY.EQ.1) Y=0.	001110
	IF(JY.EQ.2) Y=.2	001120
	IF(JY.EQ.3) Y=.4	001130
	IF(JY.EQ.4) Y=.6	001140
	IF(JY.EQ.5) Y=.8	001150
	IF(JY.EQ.6) Y=1.2	001160
	IF(JY.EQ.7) Y=1.6	001170
	IF(JY.EQ.8) Y=2.	001180
	IF(JY.EQ.9) Y=2.5	001190
	IF(JY.EQ.10) Y=3.	001200
	IF(JY.EQ.11) Y=4.	001210
	IF(JY.EQ.12) Y=6.	001220
	IF(JY.EQ.13) Y=9.	001230
	IF(JY.EQ.14) Y=10.	001240
	IF(JY.EQ.15) Y=20.	001250
	IF(JY.EQ.16) Y=30.	001260
	IF(JY.EQ.17) Y=50.	001270
	Y1(JY)=Y	001280
	BL=-2./Z	001290
	IF(BL.LT.-20.) BL=-20.	001300
	BU=-BL	001310
	IELE=1	001320
	CALL GAUSS(MX,1,20,1,1.E-3,1.E-3,BL,BU,GINT,ICALC,TEMP1,FX)	001330
	DO 5 IX=1,MX	001340
	FI(IX,JY)=GINT(IX)	001350
5	CONTINUE	001360
4	CONTINUE	001370

	DO 6 IX=1,MX	001380
	DO 8 IY=1,MY	001390
8	FIY(IY)=FI(IX,IY)	001400
	CALL YINT(FIY,Y1,SIG1,MY)	001410
	IF(IS.EQ.1) STRSS(1,1,IX)=SIG1	001420
	IF(IS.EQ.2) STRSS(2,2,IX)=SIG1	001430
	IF(IS.EQ.3) STRSS(3,3,IX)=SIG1	001440
	IF(IS.EQ.4) STRSS(1,2,IX)=STRSS(2,1,IX)=SIG1	001450
	IF(IS.EQ.5) STRSS(2,3,IX)=STRSS(3,2,IX)=SIG1	001460
	IF(IS.EQ.6) STRSS(1,3,IX)=STRSS(3,1,IX)=SIG1	001470
6	CONTINUE	001480
9	CONTINUE	001490
	RETURN	001500
10	CONTINUE	001510
	DO 12 ISTRSS=1,5	001520
	IS=ISTRSS	001530
	DO 11 IX=1,MX	001540
	X=X1(IX,1)	001550
	XK1=(1.+X)**2+Z**2	001560
	XK2=(1.-X)**2+Z**2	001570
	C1=SQRT(XK2/XK1)	001580
	C2=SQRT(2.*C1*(XK1+XK2-4.)/XK1)	001590
	SI=PI/XK1*(1.-C1)/C1/C2	001600
	SIB=PI/XK1*(1.+C1)/C1/C2	001610
	SXN=-1./PI*Z*((1.+2.*X**2+2.*Z**2)*SIB-2.*PI-3.*X*SI)	001620
	SZN=-Z/PI*(SIB-X*SI)	001630
	TXZN=-1./PI*Z**2*SI	001640
	CTZ=-1./PI*((1.+2.*X**2+2.*Z**2)*Z*SIB-2.*PI*Z-3.*X*Z*SI)	001650
	TXZT=FT*CTZ	001660
	TYZT=FA*CTZ	001670
	CXT=-1./PI*((2.*X**2-2.-3.*Z**2)*SI+2.*PI*X+2.*(1.-X**2-Z**2)*X	001680
	1*SIB)	001690
	SXT=FT*CXT	001700
	SYT=FA*CXT	001710
	SZT=-((FT+FA)/PI*Z**2*SI	001720
	IF(IS.EQ.1) STRSS(1,1,IX)=SXN+SXT	001730
	IF(IS.EQ.2) STRSS(2,2,IX)=GNU*(SXN+SXT+SZN+SZT)+SYT	001740
	IF(IS.EQ.3) STRSS(3,3,IX)=SZN+SZT	001750
	IF(IS.EQ.4) STRSS(1,2,IX)=STRSS(2,1,IX)=0.	001760
	IF(IS.EQ.5) STRSS(2,3,IX)=STRSS(3,2,IX)=TYZT	001770
	IF(IS.EQ.6) STRSS(1,3,IX)=STRSS(3,1,IX)=TXZN+TXZT	001780
11	CONTINUE	001790
12	CONTINUE	001800
	RETURN	001810
	END	001820
	SUBROUTINE YINT(FI,Y1,SIG1,MY)	001830
	DIMENSION FI(17),Y1(17)	001840
	C1=FI(1)*(Y1(2)-Y1(1))	001850
	C2=FI(MY)*(Y1(MY)-Y1(MY-1))	001860
	SUM=0.	001870
	MY1=MY-1	001880
	DO 1 I=2,MY1	001890
1	SUM=SUM+FI(I)*(Y1(I+1)-Y1(I-1))	001900
	SIG1=C1+C2+SUM	001910
	RETURN	001920
	END	001930
	SUBROUTINE FEVAL(X,FX,JF,ICALC)	001940
	COMMON/F/ ISTRSS,X1(22,1),GNU,Z0,Y,XK,FT,FA,MX	001950
	DIMENSION FX(22),ICALC(22)	001960
	PI=3.14159	001970
	X2=X**2	001980
	Y2=Y**2	001990
	GNU1=1.-2.*GNU	002000

	R=SQRT(X**2+Y**2+1.)	002010
	R2=R**2	002020
	R3=R**3	002030
	R5=R**5	002040
	RZ=R+1.	002050
	IF(ISTRSS.EQ.1) 1,2	002060
1	C1=(GNU1/R3-3.*X2/R5-GNU1/R/RZ*(1.-X2/R/RZ-X2/R2))/2./PI	002070
	C2=(GNU1/R3-3.*X2/R5-GNU1/R/RZ**2*(3.-X2*(3.*R+1.)/R2/RZ))/2./PI*X	002080
	C3=0.	002090
	GO TO 10	002100
2	IF(ISTRSS.EQ.2) 3,4	002110
3	C1=(GNU1/R3-3.*Y2/R5-GNU1/R/RZ*(1.-Y2/R/RZ-Y2/R2))/2./PI	002120
	C2=(GNU1/R3-3.*Y2/R5-GNU1/R/RZ**2*(1.-Y2*(3.*R+1.)/R2/RZ))*X/2./PI	002130
	C3=0.	002140
	GO TO 10	002150
4	IF(ISTRSS.EQ.3) 5,6	002160
5	C1=-3./R5/2./PI	002170
	C2=-3./2./PI*X/R5	002180
	C3=0.	002190
	GO TO 10	002200
6	IF(ISTRSS.EQ.4) 7,8	002210
7	C1=0.	002220
	C2=0.	002230
	C3=(-3.*X2/R5-GNU1/R/RZ**2*(1.-X2*(3.*R+1.)/R2/RZ))/2./PI*X	002240
	GO TO 10	002250
8	IF(ISTRSS.EQ.5) 9,11	002260
9	C1=0.	002270
	C2=0.	002280
	C3=-3./2./PI*Y2/R5	002290
	GO TO 10	002300
11	C1=-3./2./PI*X/R5	002310
	C2=-3./2./PI*X2/R5	002320
	C3=0.	002330
10	ARG=C1+FY*C2+FX*C3	002340
	DO 14 I=1,JF	002350
	IF(ICALC(I))14,13,13	002360
13	CONTINUE	002370
	ARGU=1.-(ZB*X-X1(I,1))**2-(ZB*Y*YK)**2	002380
	IF(ARGU.LT.0.) 15,16	002390
15	FY(I)=1.E-12	002400
	GO TO 17	002410
16	CONTINUE	002420
	FX(I)=SORT(ARGU)*ARG	002430
17	CONTINUE	002440
14	CONTINUE	002450
	RETURN	002460
	END	002470
	SUBROUTINE PRINC(STRSS,IX,SH,SIN,SMN)	002480
	DIMENSION STRSS(3,3,22)	002490
	C1=STRSS(1,1,IX)+STRSS(2,2,IX)+STRSS(3,3,IX)	002500
	C1=C1	002510
	C2=STRSS(1,1,IX)*STRSS(2,2,IX)+STRSS(1,1,IX)*STRSS(3,3,IX)+	002520
	1STRSS(2,2,IX)*STRSS(3,3,IX)-STRSS(1,2,IX)**2-	002530
	2STRSS(1,3,IX)**2-STRSS(2,3,IX)**2	002540
	C3=STRSS(1,1,IX)*STRSS(2,2,IX)+STRSS(3,3,IX)+	002550
	12.*STRSS(1,2,IX)*STRSS(2,3,IX)+STRSS(1,3,IX)-	002560
	2STRSS(1,1,IX)*STRSS(2,3,IX)**2-	002570
	3STRSS(2,2,IX)*STRSS(1,3,IX)**2-	002580
	4STRSS(3,3,IX)*STRSS(1,2,IX)**2	002590
	C3=C3	002600
	CALL CUBIC(C1,C2,C3,S1,S2,S3)	002610
	SM=S1	002620
	IF(S2.GT.SM) SM=S2	002630

	IF(S3.GT.SM) SM=S3	002640
	SMN=S1	002650
	IF(S2.LT.SMN) SMN=S2	002660
	IF(S3.LT.SMN) SMN=S3	002670
	SIM=S1	002680
	IF(S2.GT.SMN.AND.S2.LT.SM) SIM=S2	002690
	IF(S3.GT.SMN.AND.S3.LT.SM) SIM=S3	002700
	RETURN	002710
	END	002720
	SUBROUTINE CUBIC(C1,C2,C3,S1,S2,S3)	002730
	PI=3.14159	002740
	A=1./3.*(3.*C2-C1**2)	002750
	B=1./27.*(2.*C1**3-9.*C1*C2+27.*C3)	002760
	IF(A.LT.0.) GO TO 3	002770
	S1=S2=S3=0.	002780
	RETURN	002790
3	CONTINUE	002800
	PHI=ACOS((-B/2./SQRT(-A**3/27.))	002810
	S1=2.*SQRT(-A/3.)*COS(PHI/3.)-C1/3.	002820
	S2=2.*SQRT(-A/3.)*COS(PHI/3.+2.*PI/3.)-C1/3.	002830
	S3=2.*SQRT(-A/3.)*COS(PHI/3.+4.*PI/3.)-C1/3.	002840
	RETURN	002850
	END	002860
	SUBROUTINE ANGLP(STRSS,S1,S2,S3,AN,IX,SIGNA)	002870
	DIMENSION STRSS(3,3,22),AN(3,3)	002880
	S11=STRSS(1,1,IX)	002890
	S12=STRSS(1,2,IX)	002900
	S13=STRSS(1,3,IX)	002910
	S22=STRSS(2,2,IX)	002920
	S23=STRSS(2,3,IX)	002930
	S33=STRSS(3,3,IX)	002940
	ER=1.E-3	002950
	DO 2 I=1,3	002960
	IF(I.EQ.1) S=S1	002970
	IF(I.EQ.2) S=S2	002980
	IF(I.EQ.3) S=S3	002990
	IF(ABS(S11-S).LT.ER) 3,4	003000
3	AN(I,1)=1.	003010
	AN(I,2)=AN(I,3)=0.	003020
	GO TO 14	003030
4	IF(ABS(S22-S).LT.ER) 5,6	003040
5	AN(I,2)=1.	003050
	AN(I,1)=AN(I,3)=0.	003060
	GO TO 14	003070
6	IF(ABS(S33-S).LT.ER) 7,8	003080
7	AN(I,3)=1.	003090
	AN(I,1)=AN(I,2)=0.	003100
	GO TO 14	003110
8	IF(ABS(S12).LT.ER.AND.ABS(S13).LT.ER) 9,10	003120
10	A=(-(S12*S13-(S11-S)*S23)/(S12**2-(S11-S)*(S22-S))	003130
	C11=(((-S12*A-S13)/(S11-S))**2+1.+A**2	003140
	AN(I,3)=SIGNA*SQRT(1./C11)	003150
	AN(I,2)=A*AN(I,3)	003160
	AN(I,1)=(-S12*AN(I,2)-S13*AN(I,3))/(S11-S)	003170
	GO TO 14	003180
9	IF(ABS(S12).LT.ER.AND.ABS(S23).LT.ER) 11,12	003190
11	A=(-(S12*S23-(S22-S)*S13)/(S23**2-(S22-S)*(S33-S))	003200
	C11=(((-S12*S23-A)/(S22-S))**2+1.+A**2	003210
	AN(I,1)=SIGNA*SQRT(1./C11)	003220
	AN(I,3)=A*AN(I,1)	003230
	AN(I,2)=(-S23*AN(I,3)-S12*AN(I,1))/(S22-S)	003240
	GO TO 14	003250
12	CONTINUE	003260

	A=(-S13*S23-S12*(S33-S1))/(S13**2-(S11-S)*(S33-S1))	003270
	C11=((-S23-S13*A)/(S33-S1))**2+1.+A**2	003280
	AN(I,2)=SIGN*SQRT(1./C11)	003290
	AN(I,1)=A*AN(I,2)	003300
14	AN(I,3)=(-S13*AN(I,1)-S23*AN(I,2))/(S33-S)	003310
2	CONTINUE	003320
	CONTINUE	003330
	RETURN	003340
	END	003350
	SUBROUTINE RVSTRS(STRSS,AN,AS,TRM,TMXX,I,SIGN)	003360
	COMMON/F/ ISTRSS,X1(22,1),GNU,ZR,Y,XK,FT,FA,MX	003370
	DIMENSION STRSS(3,3,22),AN(3,22),AS(3,22)	003380
	TRM=0.	003390
	TMXX=0.	003400
	EP=1.E-3	003410
	DO 1 IAS=1,21	003420
	AS1=-1.+1.*FLOAT(IAS-1)	003430
	IF(ABS(AN(2,I)).LT.ER.AND.ABS(AN(1,I)).LT.ER) 8,9	003440
8	AS3=0.	003450
	AS2=SIGN*SQRT(1.-AS1**2)	003460
	GO TO 13	003470
9	IF(ABS(AN(1,I)).LT.ER.AND.ABS(AN(3,I)).LT.ER) 10,11	003480
10	AS2=0.	003490
	AS3=SIGN*SQRT(1.-AS1**2)	003500
	GO TO 13	003510
11	IF(ABS(AN(2,I)).LT.ER.AND.ABS(AN(3,I)).LT.ER) GO TO 12	003520
	IF(ABS(AN(2,I)).LT.ER) 16,17	003530
16	AS3=-AN(1,I)*AS1/AN(3,I)	003540
	CC=1.-AS1**2-AS3**2	003550
	IF(CC.LT.0.) GO TO 22	003560
	AS2=SIGN*SQRT(CC)	003570
	GO TO 13	003580
17	IF(ABS(AN(3,I)).LT.ER) 18,19	003590
18	AS2=-AS1*AN(1,I)/AN(2,I)	003600
	CC=1.-AS1**2-AS2**2	003610
	IF(CC.LT.0.) GO TO 22	003620
	AS3=SIGN*SQRT(CC)	003630
	GO TO 13	003640
19	IF(ABS(AN(1,I)).LT.ER) 20,21	003650
20	AS2=AN(3,I)*SIGN*SQRT(1.-AS1**2)	003660
	AS3=-AN(2,I)/AN(3,I)*AS2	003670
	GO TO 13	003680
21	A=AN(2,I)**2+AN(3,I)**2	003690
	B=2.*AN(1,I)*AN(3,I)*AS1	003700
	C=AS1**2+AN(1,I)**2+AN(2,I)**2+AS1**2-AN(2,I)**2	003710
	CC=B**2-4.*A*C	003720
	IF(CC.LT.0.) GO TO 22	003730
	AS3=(-B+SIGN*SQRT(CC))/2./A	003740
	AS2=-((AS3*AN(3,I)+AS1*AN(1,I))/AN(2,I)	003750
13	CONTINUE	003760
	TMX=-1.E+20	003770
	TMN=1.E+20	003780
	DO 2 IX=1,MX	003790
	TAU=AN(1,I)*AS1*STRSS(1,1,IX)+AN(2,I)*AS2*STRSS(2,2,IX)	003800
	1+AN(3,I)*AS3*STRSS(3,3,IX)+AN(1,I)*AS2*STRSS(1,2,IX)	003810
	2+AN(2,I)*AS1*STRSS(1,2,IX)+AN(1,I)*AS3*STRSS(1,3,IX)	003820
	3+AN(3,I)*AS1*STRSS(1,3,IX)+AN(2,I)*AS3*STRSS(2,3,IX)	003830
	4+AN(3,I)*AS2*STRSS(2,3,IX)	003840
	IF(TAU.GT.TMX) 3,4	003850
3	TMX=TAU	003860
	AST1=AS1	003870
	AST2=AS2	003880
	AST3=AS3	003890

4	IF(TAU.LT.TMN) 5,6	003900
5	TMN=TAU	003910
6	CONTINUE	003920
2	CONTINUE	003930
	TRV=TMX-TMN	003940
	IF(ABS(TRV).GT.ABS(TVM)) TRVM=TRV	003950
	IF(ABS(TMN).GT.ABS(TMX)) TMX=ABS(TMN)	003960
	IF(TMX.GT.TMXX) 23,22	003970
23	TMXX=TMX	003980
	AS(1,I)=AST1	003990
	AS(2,I)=AST2	004000
	AS(3,I)=AST3	004010
22	CONTINUE	004020
1	CONTINUE	004030
	RETURN	004040
12	WRITE(1,15)	004050
15	FORMAT(* SOLUTION NOT APPROPRIATE *)	004060
	RETURN	004070
	END	004080
	SUBROUTINE ANGTRAN(AN,BN,CN,IX)	004090
	DIMENSION AN(3,3),BN(3),CN(3,22)	004100
	CN(1,IX)=BN(1)*AN(1,1)+BN(2)*AN(2,1)+BN(3)*AN(3,1)	004110
	CN(2,IX)=BN(1)*AN(1,2)+BN(2)*AN(2,2)+BN(3)*AN(3,2)	004120
	CN(3,IX)=BN(1)*AN(1,3)+BN(2)*AN(2,3)+BN(3)*AN(3,3)	004130
	RETURN	004140
	END	004150
	SUBROUTINE XPOS	004160
	COMMON/F/ IS,X1(22,1),GNU,Z,Y,XK,FI,FA,MX	004170
	IF(MX.EQ.7) 1,2	004180
1	X1(1,1)=-.8	004190
	X1(2,1)=-.5	004200
	X1(3,1)=-.3	004210
	X1(4,1)=0.	004220
	X1(5,1)=.3	004230
	X1(6,1)=.5	004240
	X1(7,1)=.8	004250
	RETURN	004260
2	IF(MX.EQ.11) 3,4	004270
3	X1(1,1)=-1.	004280
	X1(2,1)=-.9	004290
	X1(3,1)=-.8	004300
	X1(4,1)=-.5	004310
	X1(5,1)=-.3	004320
	X1(6,1)=0.	004330
	X1(7,1)=.3	004340
	X1(8,1)=.5	004350
	X1(9,1)=.6	004360
	X1(10,1)=.9	004370
	X1(11,1)=1.	004380
	RETURN	004390
4	IF(MX.EQ.15) 5,6	004400
5	X1(1,1)=-1.	004410
	X1(2,1)=-1.	004420
	X1(3,1)=-.9	004430
	X1(4,1)=-.8	004440
	X1(5,1)=-.7	004450
	X1(6,1)=-.5	004460
	X1(7,1)=-.3	004470
	X1(8,1)=0.	004480
	X1(9,1)=.3	004490
	X1(10,1)=.5	004500
	X1(11,1)=.7	004510
	X1(12,1)=.8	004520

X1(13,1)=.9
X1(14,1)=1.
X1(15,1)=1.1
RETURN

004530
004540
004550
004560
004570
004580
004590
004600

6 PRINT 10
10 FORMAT(* MATRIX NOT AVAILABLE *)
RETURN
END